THE ASTROPHYSICAL JOURNAL SUPPLEMENT SERIES, 58:341–378, 1985 July

MOLECULAR LINE SURVEY OF ORION A FROM 215 TO 247 GHz

E. C. SUTTON,[1,2] GEOFFREY A. BLAKE,[3] C. R. MASSON,[1] AND T. G. PHILLIPS[1]
Received 1984 September 13; accepted 1984 December 17

ABSTRACT

Molecular line emission from the core of the Orion molecular cloud has been surveyed from 215 to 247 GHz to an average sensitivity of about 0.2 K. A total of 544 resolvable lines were detected, of which 517 are identified and attributed to 25 distinct chemical species. A large fraction of the lines are partially blended with other identified transitions. Because of the large line width in the Orion core, the spectrum is near the confusion limit for the weakest lines identified (≈ 0.2 K).

The most abundant complex molecules present are $HCOOCH_3$, CH_3OCH_3, and C_2H_5CN, with beam-averaged column densities of about 3×10^{15} cm^{-2}. Together with the simpler species SO_2, CH_3OH, and CH_3CN, they account for approximately 70% of the lines in the spectrum. Relatively few unidentified lines are present. There are 27 lines clearly present in the spectrum which are currently unidentified. However, many of these are thought to be high-lying transitions of complex asymmetric rotors such as CH_3OH. Present spectroscopic data are inadequate to predict the frequencies of such transitions with sufficient accuracy.

Subject headings: interstellar: molecules — line identifications — radio sources: lines

I. INTRODUCTION

Studies of molecular line emission have provided much of our understanding about conditions in molecular clouds. One area of investigation has been the chemistry of these regions. Progressively more complex molecules have been found over the past dozen years. We are only beginning to understand the reactions leading to the formation of these species and why in many cases they are favored over some much simpler chemical species. Other information available from the strengths of molecular lines includes indications of densities and excitation conditions present in these clouds. Further information is provided on the gas kinematics, particularly in regions such as Orion A where line widths and central velocities have helped identify several distinct components of the gas, the so-called "spike," "hot core," and "plateau" components.

To date relatively few systematic surveys of molecular line emission have been undertaken. Lovas, Snyder, and Johnson (1979) summarized the literature through 1978. Most of the observations reported were isolated studies of at most a few transitions in one or two sources. Subsequently, Hollis *et al.* (1981) among others have reported a number of additional transitions of several species. The most extensive published spectral-line survey is that which has been recently completed at the Onsala Space Observatory (Johansson *et al.* 1984). The Onsala group surveyed Orion A and IRC+10216 from 73 to 91 GHz, detecting a total of 170 and 45 lines respectively from these two sources. Also Linke, Cummins, and Thaddeus (1985) have made an extensive survey of Sgr B2 from 70 to 145 GHz.

This current survey has been conducted at much higher frequencies, where previously observations were hindered by a lack of suitable telescopes and sufficiently sensitive receivers. There are certain advantages to high-frequency studies. For observations with similar-sized telescopes, lines are generally more intense, particularly optically thin lines from spatially unresolved sources. Thus high-frequency surveys are especially sensitive to emission from compact high-excitation regions, such as the cores of hot molecular clouds. In this survey we have covered the frequency range from 215 to 247 GHz in Orion A. We detect a total of 517 resolved identifiable lines from a total of 25 molecular species. Almost half these lines are characterized by central velocities of $v_{\rm LSR} \approx 5$ km s^{-1} and widths of about 10 km s^{-1}, typical of the dense ($n \approx 10^7$ cm^{-3}) high-temperature ($T \approx 250$ K) region known as the hot core of Orion (Morris, Palmer, and Zuckerman 1980; Genzel *et al.* 1982). Most of the remaining lines are narrower, ~ 5 km s^{-1} wide lines with central velocities of $v_{\rm LSR} = 9$ km s^{-1} representative of the spike component of the gas, a cooler, less dense, and spatially more extended region in the molecular cloud. The majority of the line flux from the Orion core is emitted in a moderately small number of lines from gas associated with the plateau source (Zuckerman and Palmer 1975; Sutton *et al.* 1984). Here the combination of large velocity widths and large column densities of molecules, such as SO_2, which are less abundant in other parts of Orion makes this region the dominant source of flux.

II. OBSERVATIONS

The observations were obtained using the 1.3 mm spectroscopy system of the Owens Valley Radio Observatory. The 10.4 m diameter telescope gave a FWHM beamwidth of 0'.5 averaged over the 215 to 247 GHz frequency range. The superconducting tunnel junction (SIS) receiver (Sutton 1983) had a noise temperature varying from 300 to 700 K (single sideband) throughout the observing band. The receiver operated in a double-sideband mode with an IF center frequency

[1] Department of Physics, California Institute of Technology.
[2] Space Sciences Laboratory, University of California, Berkeley.
[3] Department of Chemistry, California Institute of Technology.

of 1388 MHz. Single-sideband spectra were reconstructed from the observed double-sideband spectra using a procedure described below in § III. The back end of the system was a 512 channel broad-band AOS similar to that described by Masson (1982). The AOS channel width of 1.03 MHz gave a spectral resolution of 1.3 km s^{-1} in this frequency band. The observations were centered on a nominal source position of $\alpha(1950) = 05^h32^m47^s$, $\delta(1950) = -05°24'21''$.

Data were obtained on nights scattered throughout the 1982–1983 and 1983–1984 winter observing seasons. Observations from a total of 20 nights were included in the final data set. Since the requirements for atmospheric transparency were less critical than for other observing programs, some of the data were from nights of moderately high opacity ($\tau \approx 0.5$). A total of 79 double-sideband spectra comprise the data base. Integration times were typically 1000 s per spectrum for an rms noise level of about 0.2 K per resolution element.

Absolute calibration of the double-sideband spectra was done using standard "chopper wheel" techniques. Uncertainties in calibration are caused by imperfections in the sideband balance and higher-order corrections in the chopper-wheel technique. Such uncertainties amount to $\pm 15\%$. Because the emission lines arise from different-sized regions in Orion, it is not possible to correct for beam efficiency in a way which will treat all lines properly. Consequently the temperature scale has been corrected for the efficiency on extended sources (main beam plus inner sidelobes), $\eta \approx 0.85$. The brightness temperatures for spatially compact line emission are therefore systematically underestimated.

The procedure for separating sidebands (§ III) improves the accuracy of the calibration. Since each line is observed in several spectra, the observed line strengths are used to correct the relative calibration. In general the relative calibration is much better ($\leq 5\%$) over small ~ 1 GHz intervals in the spectrum and deteriorates to the original $\pm 15\%$ uncertainty over intervals greater than about 5 GHz.

III. ANALYSIS

a) Reduction to Single-Sideband Information

Each double-sideband (DSB) spectrum, considered by itself, has an unavoidable confusion as to the sideband in which each feature falls and hence its frequency. However, with a more extensive data set it is possible to avoid this ambiguity. For example, if a line is seen in one spectrum, its assignment as a lower sideband feature can be determined by whether it appears (e.g., in the upper sideband) in other appropriate spectra.

This type of analysis was automated using an algorithm similar to that used for "cleaning" aperture-synthesis maps. First the strongest feature in the entire spectrum was found, based on the naive assumption that the observed DSB temperatures were due to equal contributions from the two sidebands. Then a small fraction (~ 0.3) of the strength of this feature was subtracted from all the DSB spectra in which it should have been seen. This procedure, applied on a channel-by-channel basis (1 MHz channels), was then repeated 35,000 times until the noise level in the data was reached. A few special precautions were taken. It was necessary to treat the ends of the spectral range somewhat differently, since some frequencies there were observed in only one sideband. Also, it was necessary to treat the ^{12}CO line at 230538 MHz in a special way because of its great strength and breadth. As a result, the image sidebands of the ^{12}CO observations (approximately 227497–227543 MHz and 233453–233497 MHz) have somewhat worse signal to noise since the data folded into the ^{12}CO line have been ignored.

In order for this procedure to work it is necessary to know precisely the gains of the individual spectra. Relative gains were determined by comparing the observed strengths of the ~ 100 strongest lines in all the spectra in which they appear. Incorrect gain settings would leave false peaks (ghosts) in the image sidebands. A few false peaks as strong as about 0.5 K remain in the spectrum, implying a dynamic range of about 15–20 dB for this "cleaning" procedure.

As with any deconvolution procedure, the results are not unique. However, we have several reasons to trust the results obtained here. The convolving function is particularly simple, corresponding to a set of delta functions. Each sky frequency will appear in precisely defined places in a small number of spectra. The deconvolution is similarly straightforward, assuming the gains are well known. Ambiguities arise primarily from the treatment of the ends of the spectrum. The algorithm converges to the same result with moderate variations in parameters such as the loop gain (the amount subtracted each iteration). The vast majority of the resulting features can be identified with transitions of molecules known to exist in the interstellar medium. A few unidentified lines are present, and the strongest of these have been individually examined to confirm their presence in the original DSB data. In general, the single-sideband spectrum is thought to be trustworthy down to about 0.3 K.

b) Line Assignments

Identifications of the observed lines were made using several sources of information. Initial assignments were made using a catalog of frequencies, quantum numbers, and line strengths provided by F. J. Lovas (private communication). Also used was a revised version of the JPL catalog (Poynter and Pickett 1981). In a number of cases the existing laboratory data and predictions were insufficient for our purposes. In support of these astronomical observations, F. C. De Lucia, E. Herbst, and G. M. Plummer of Duke University undertook additional laboratory measurements of several molecules and made frequency predictions for our spectral range. Their work is the primary source of frequency data for several cases, particularly for $HCOOCH_3$.

The resulting set of line identifications and temperatures showed great uniformity. That is, the observed temperatures were consistent with the known line strengths and excitation energies. When a molecule was seen in a weak transition, it was also detected in all stronger ones.

IV. RESULTS

The reduced single-sideband spectrum is presented in Figure 1. All identified lines are indicated on the plots. Counting the components of blends separately if they can be at least partially resolved in the spectra, a total of 517 separate identified lines are present. These lines arise from 25 distinct species of interstellar molecules, not counting isotopic variants. Discussion of the results on individual molecules is contained in § V.

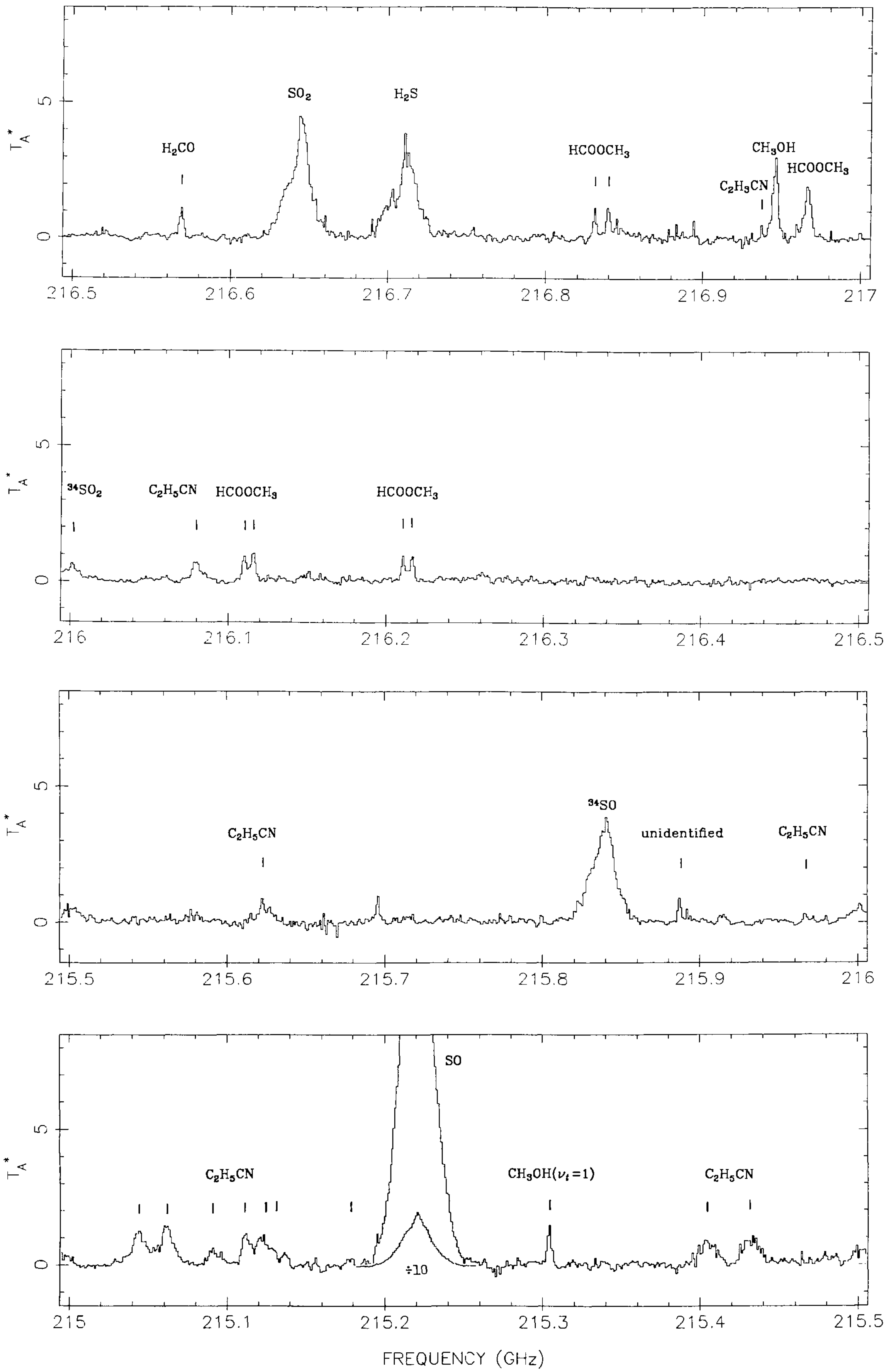

FIG. 1.—Spectrum of Orion A from 215 to 247 GHz. Antenna temperature has been corrected for an extended source efficiency of 0.85. Frequency scale is in terms of rest frequency, assuming emission from material at $v_{LSR} = 8$ km s^{-1}. Identified lines are individually marked.

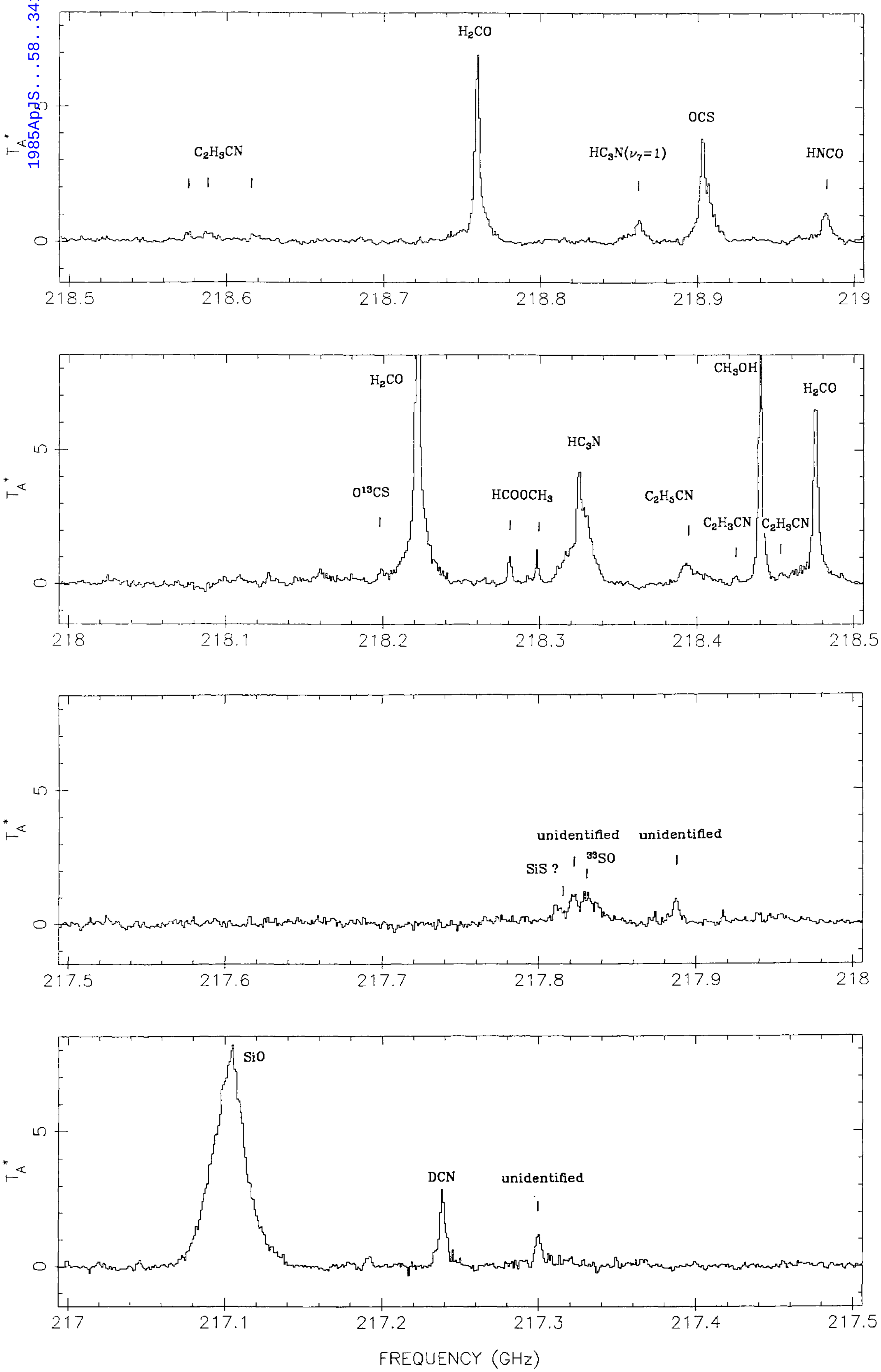

FIG. 1—*Continued*

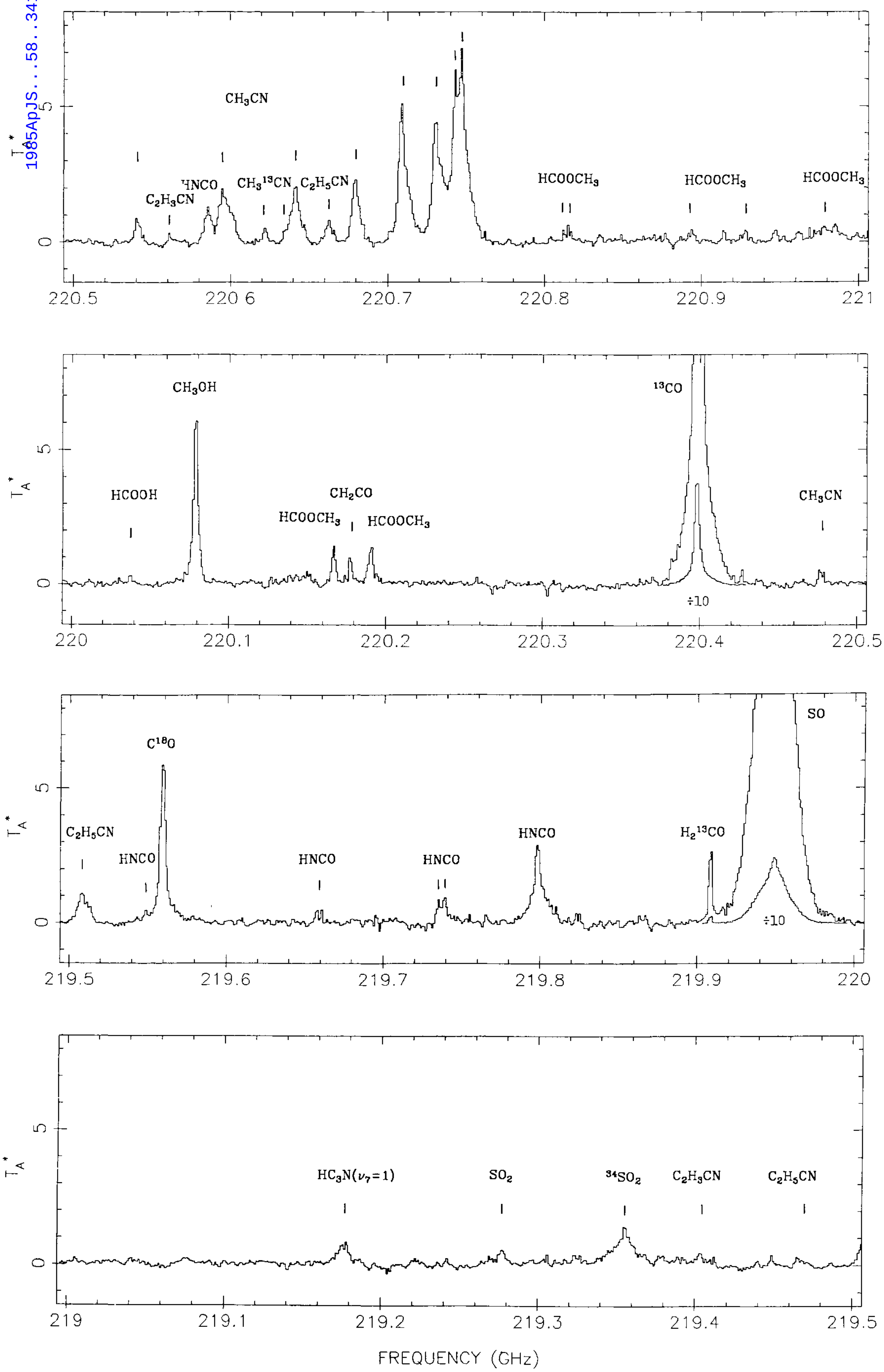

FIG. 1—*Continued*

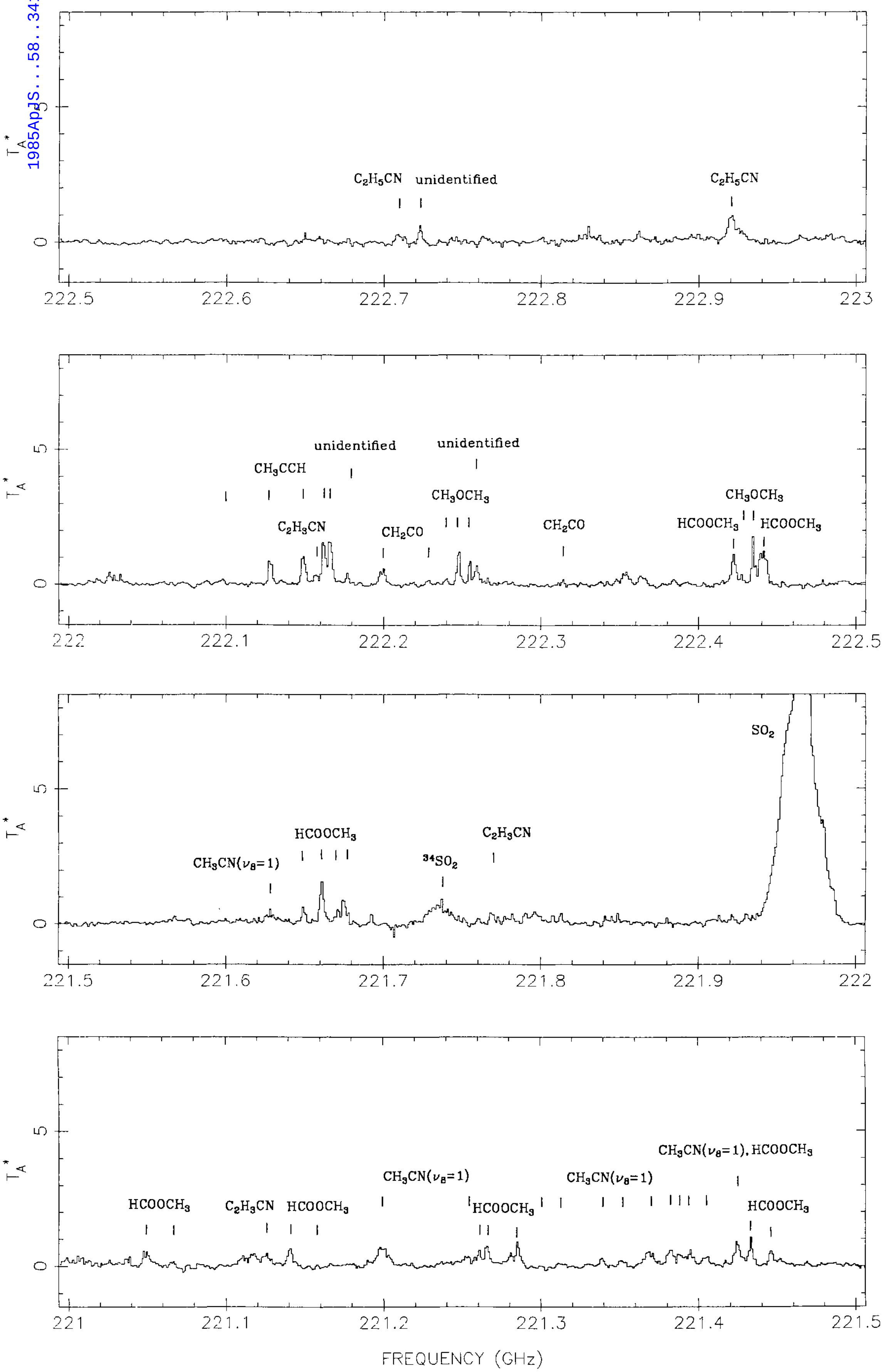

FIG. 1—*Continued*

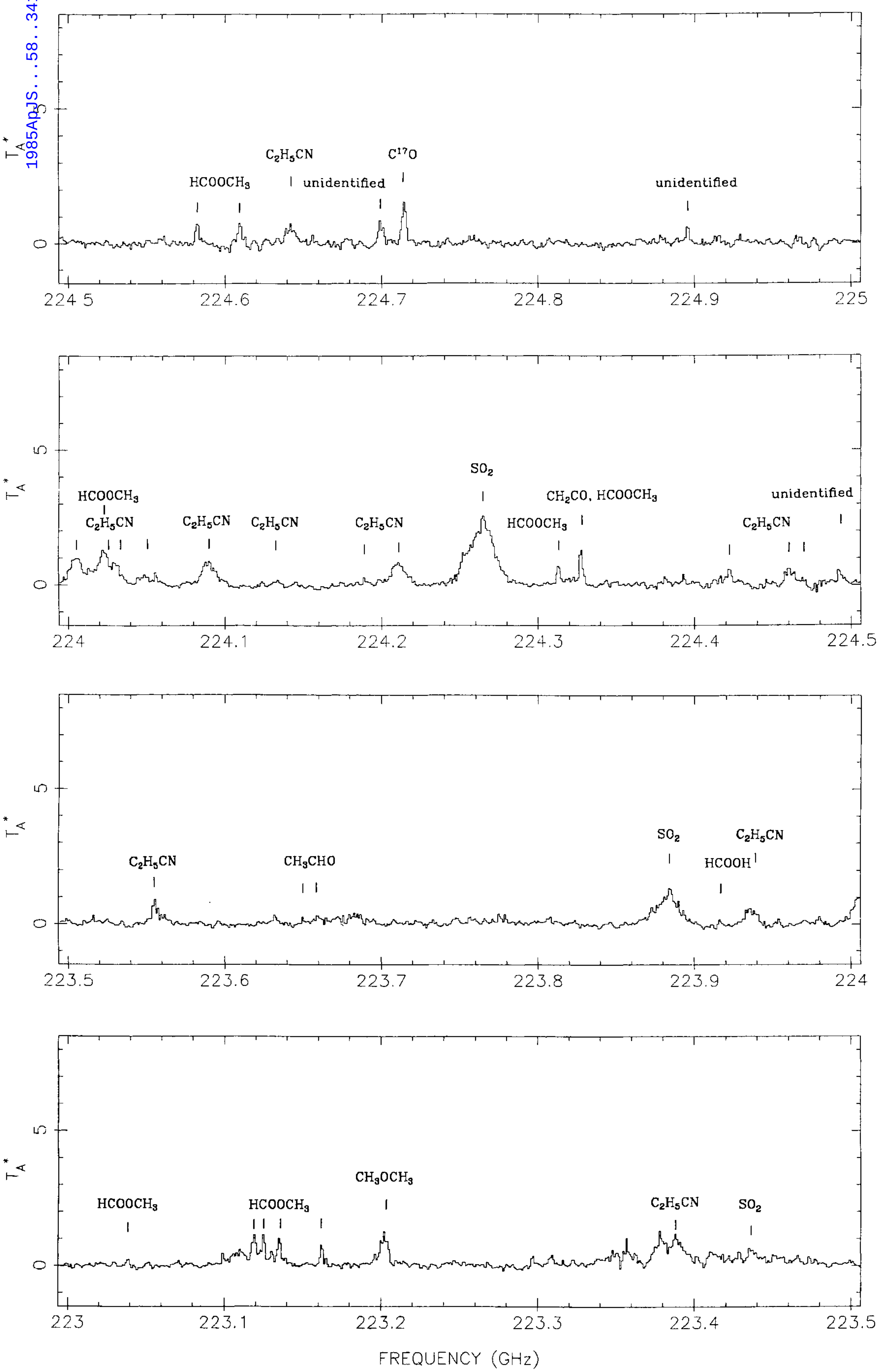

FIG. 1—*Continued*

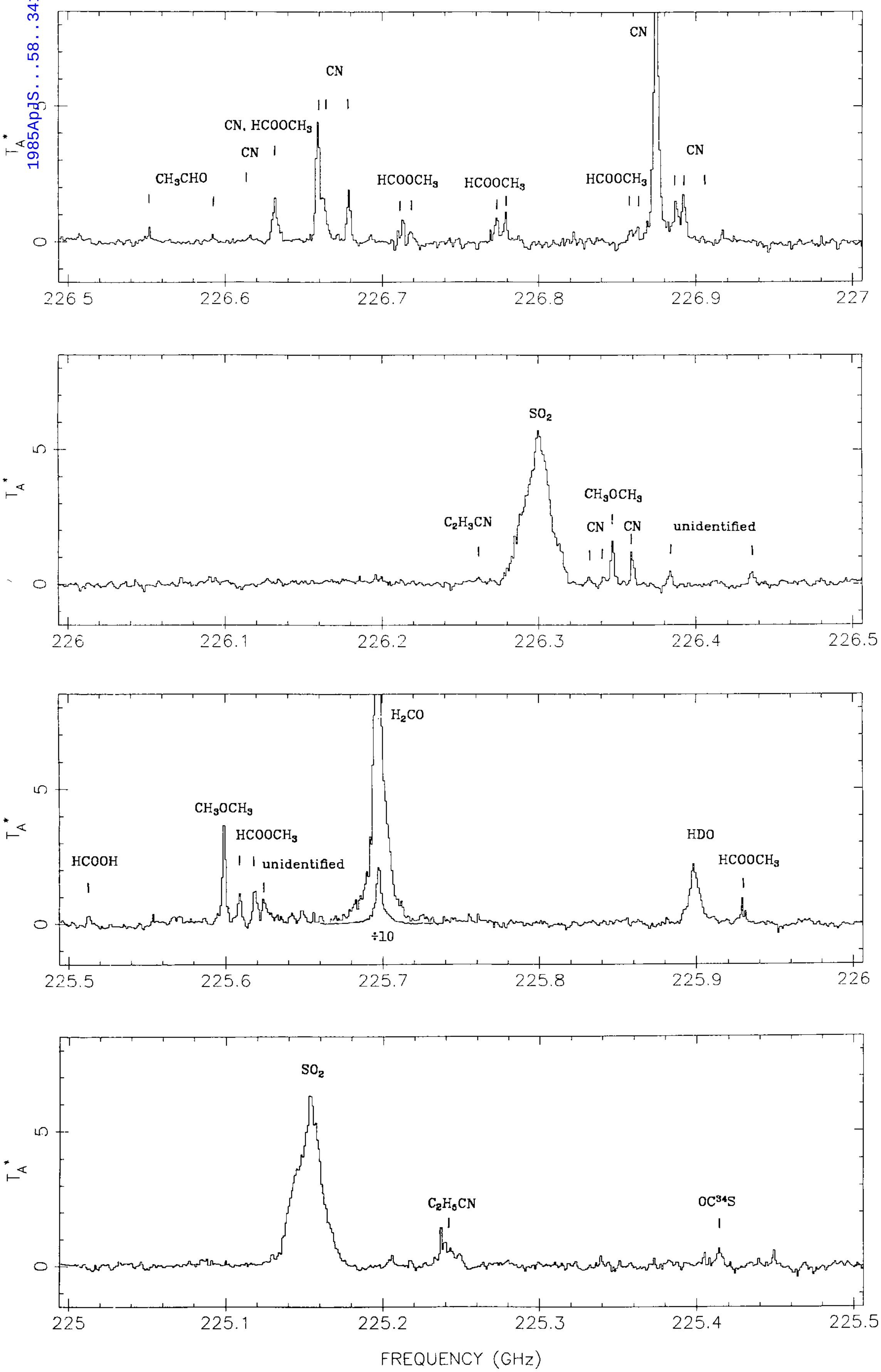

FIG. 1—*Continued*

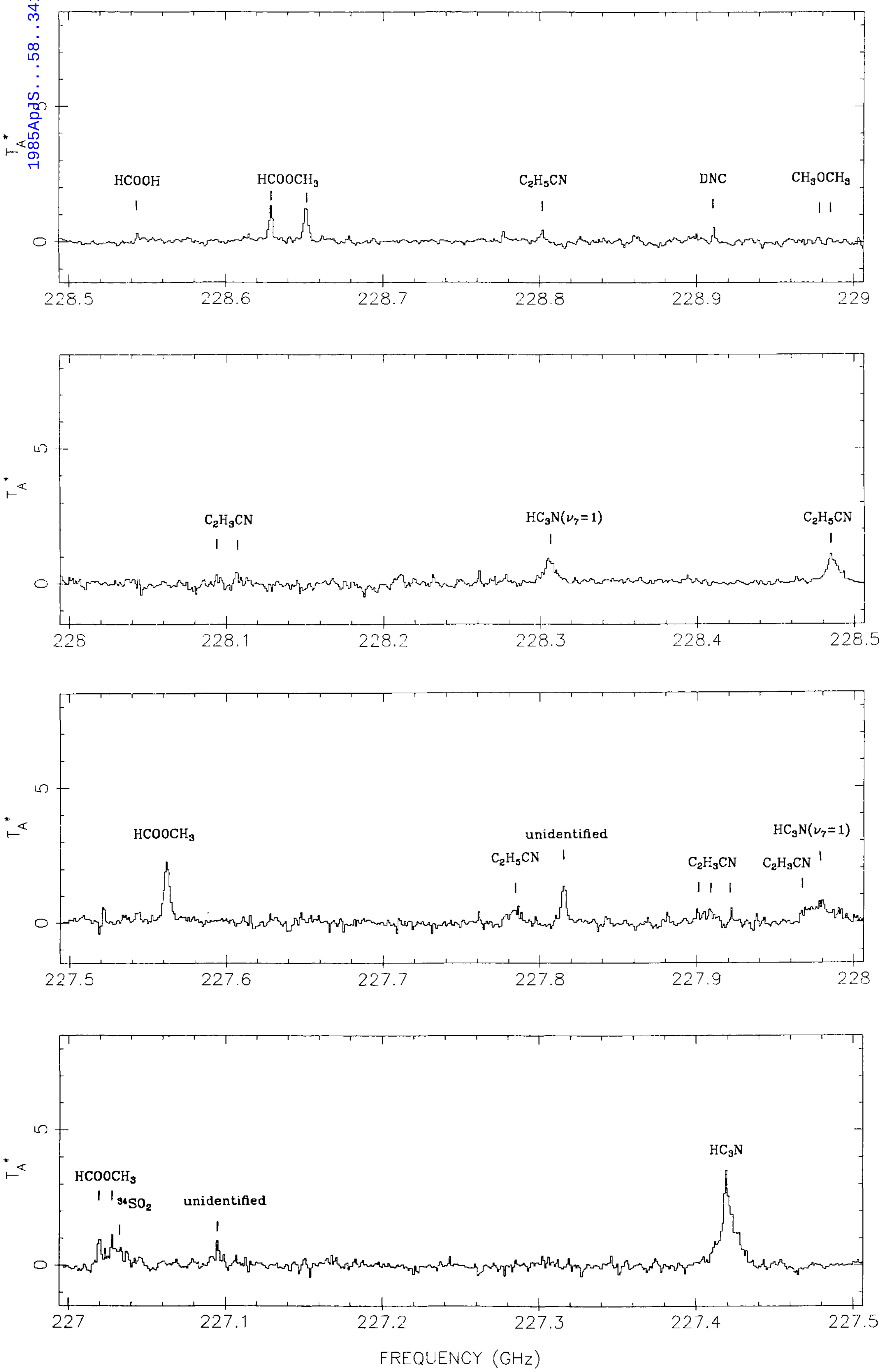

FIG. 1—*Continued*

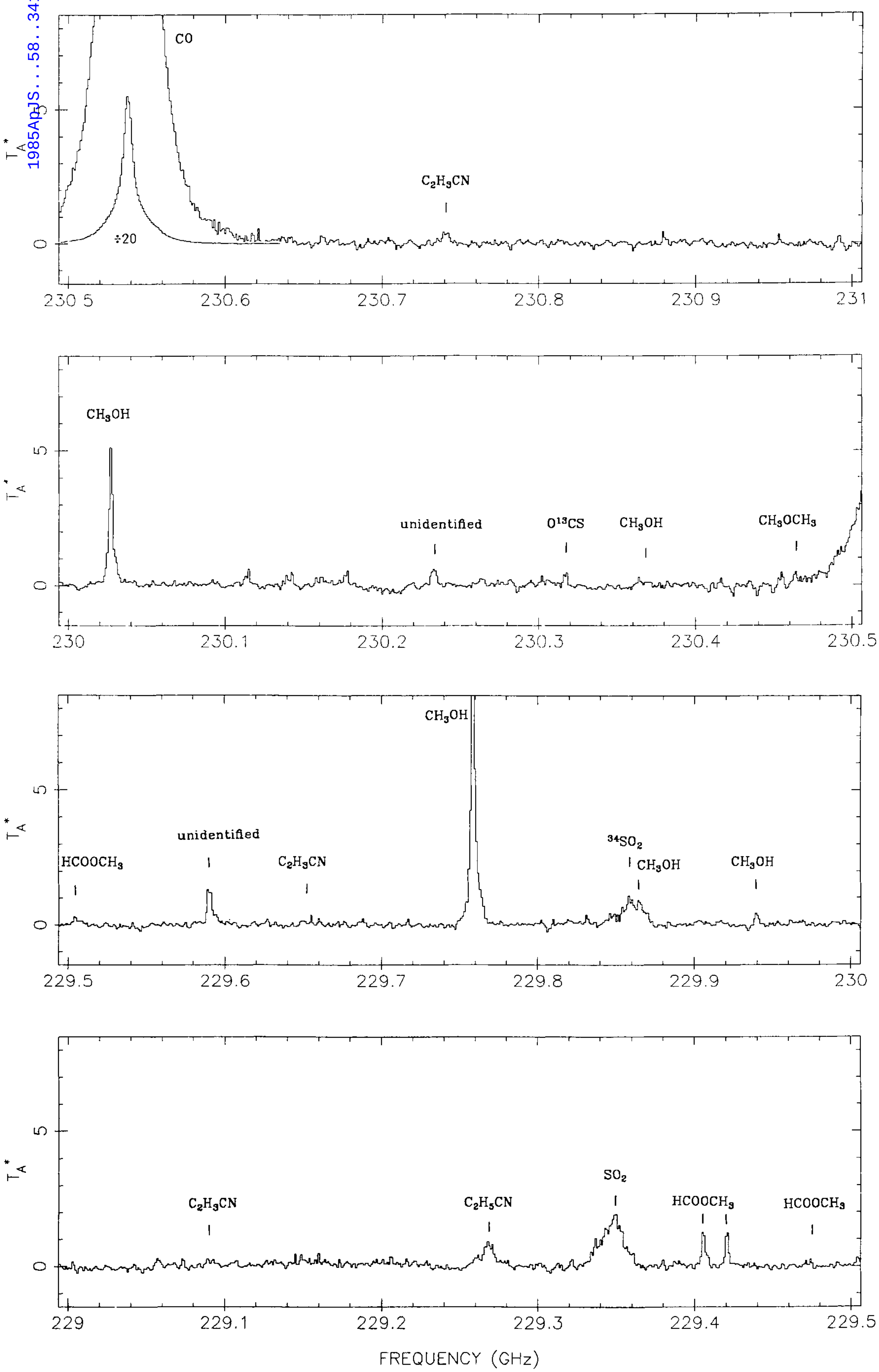

FIG. 1—*Continued*

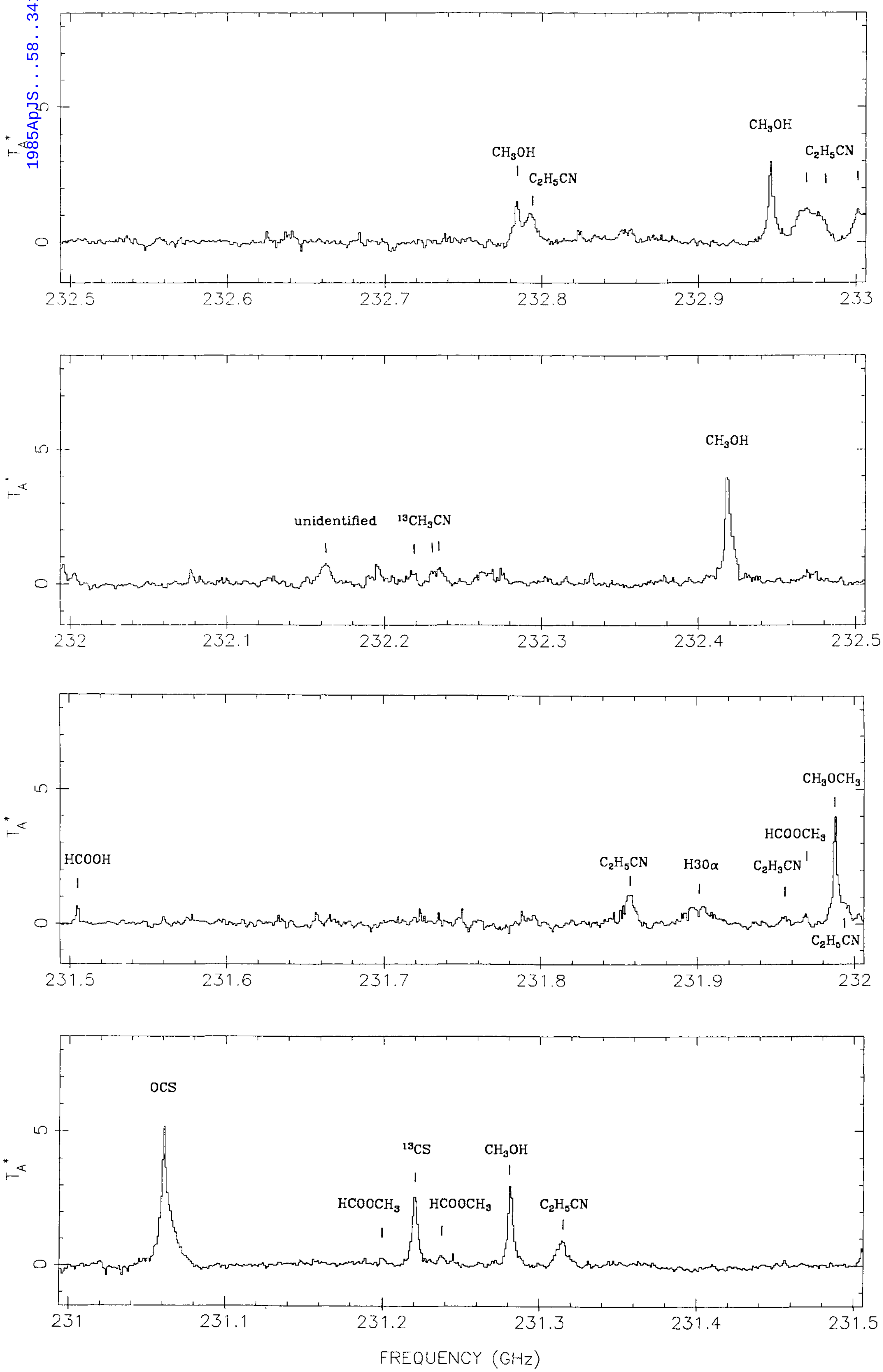

FIG. 1—*Continued*

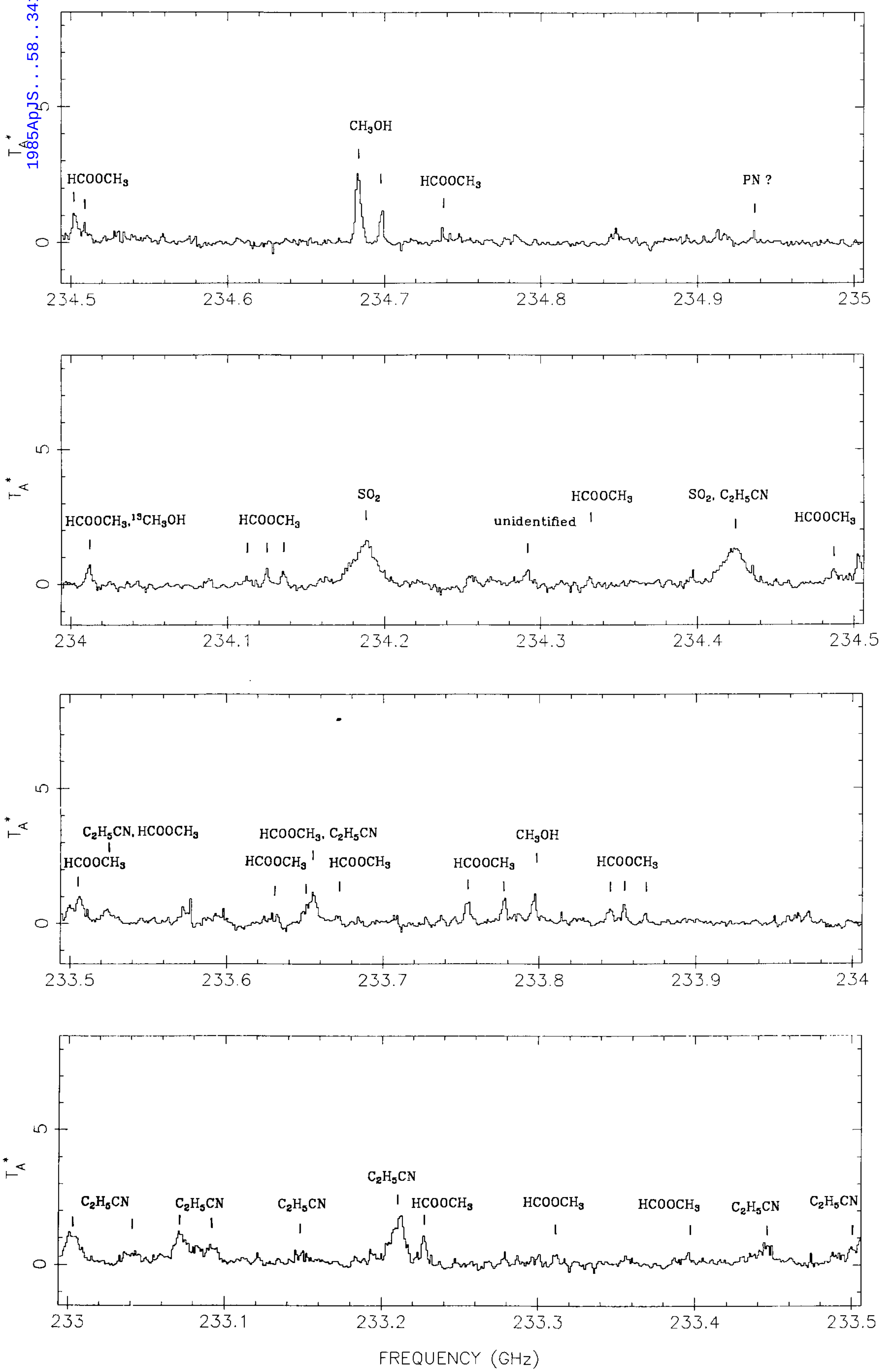

FIG. 1—*Continued*

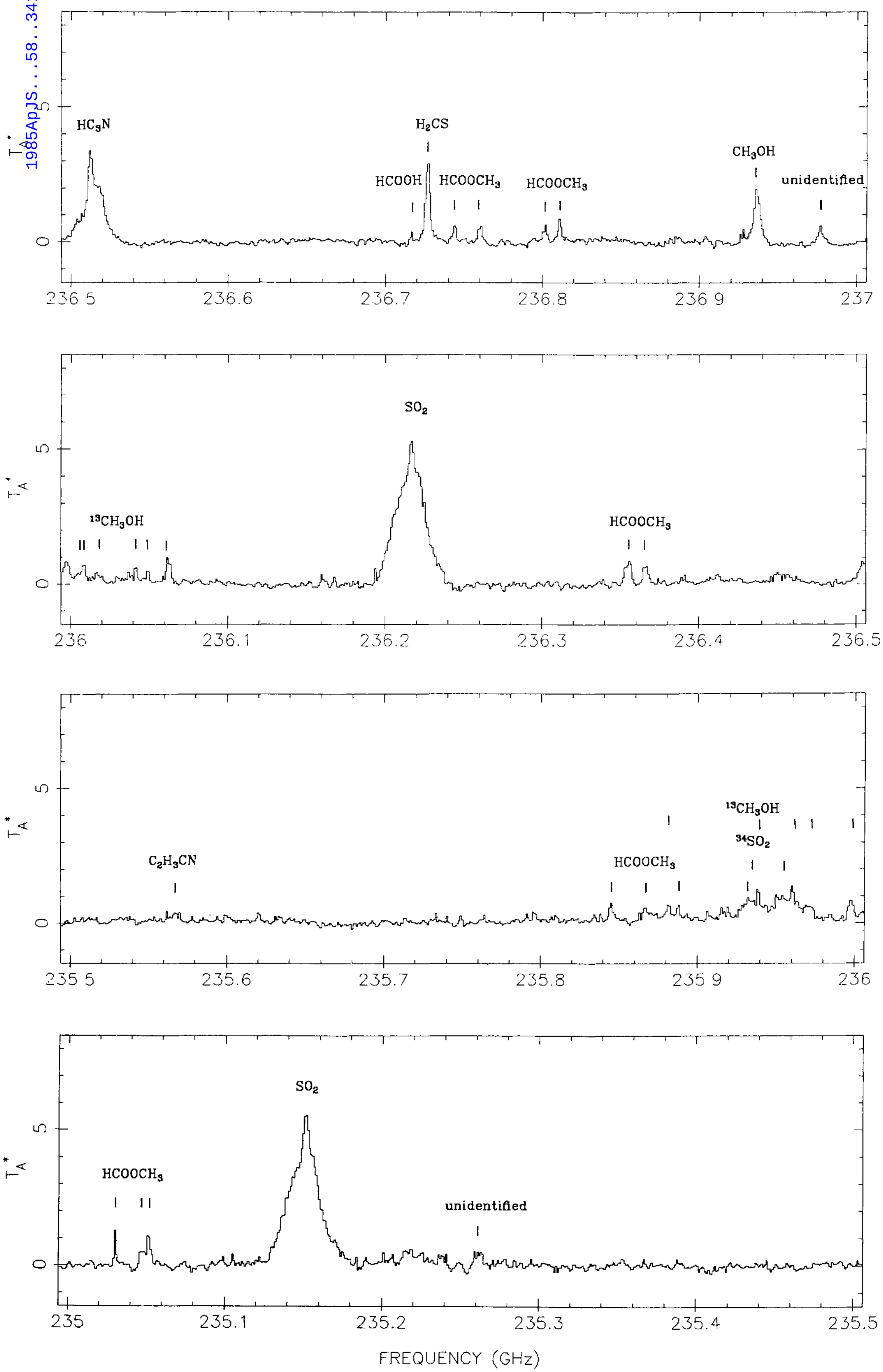

FIG. 1—*Continued*

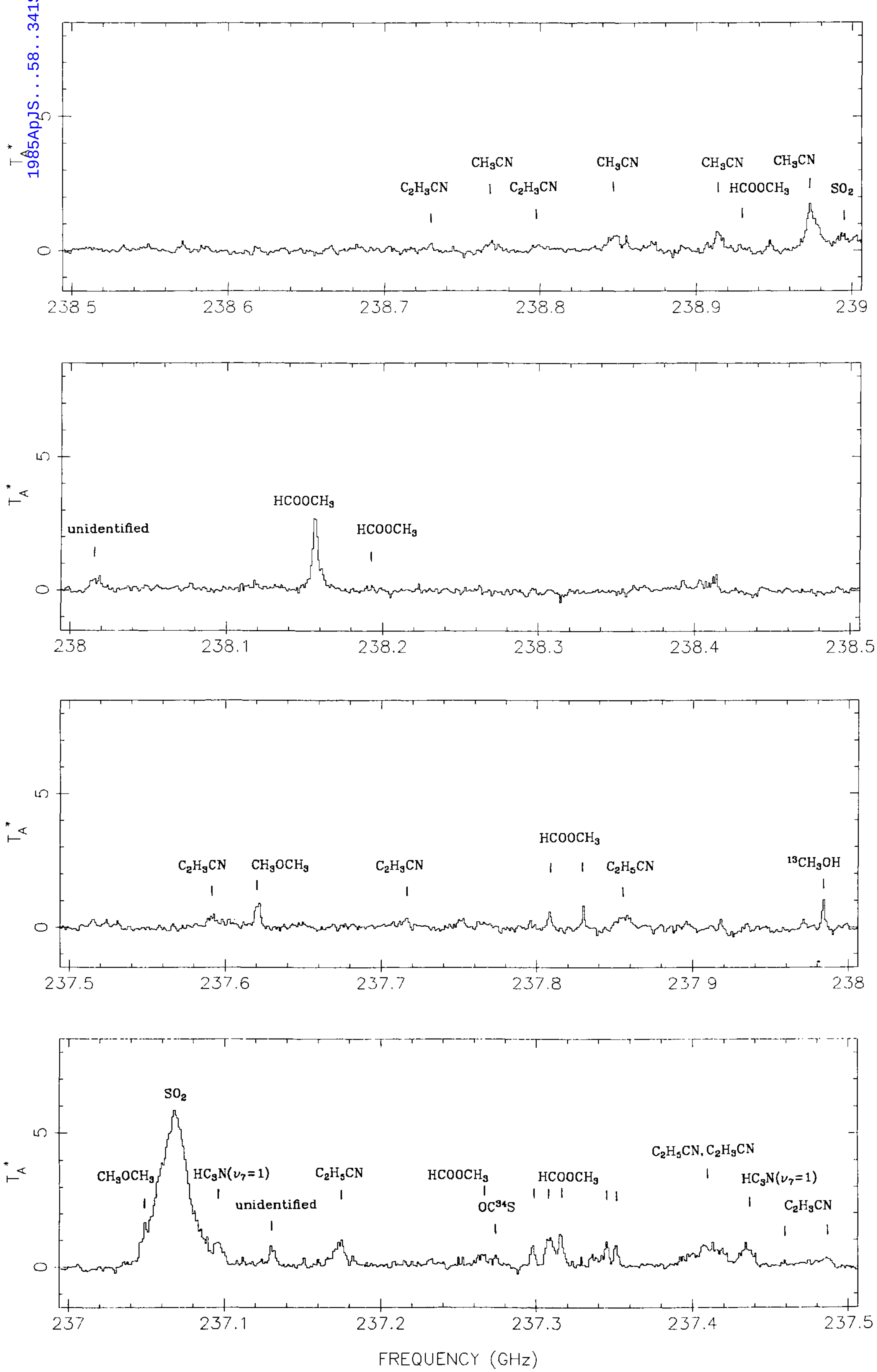

FIG. 1—*Continued*

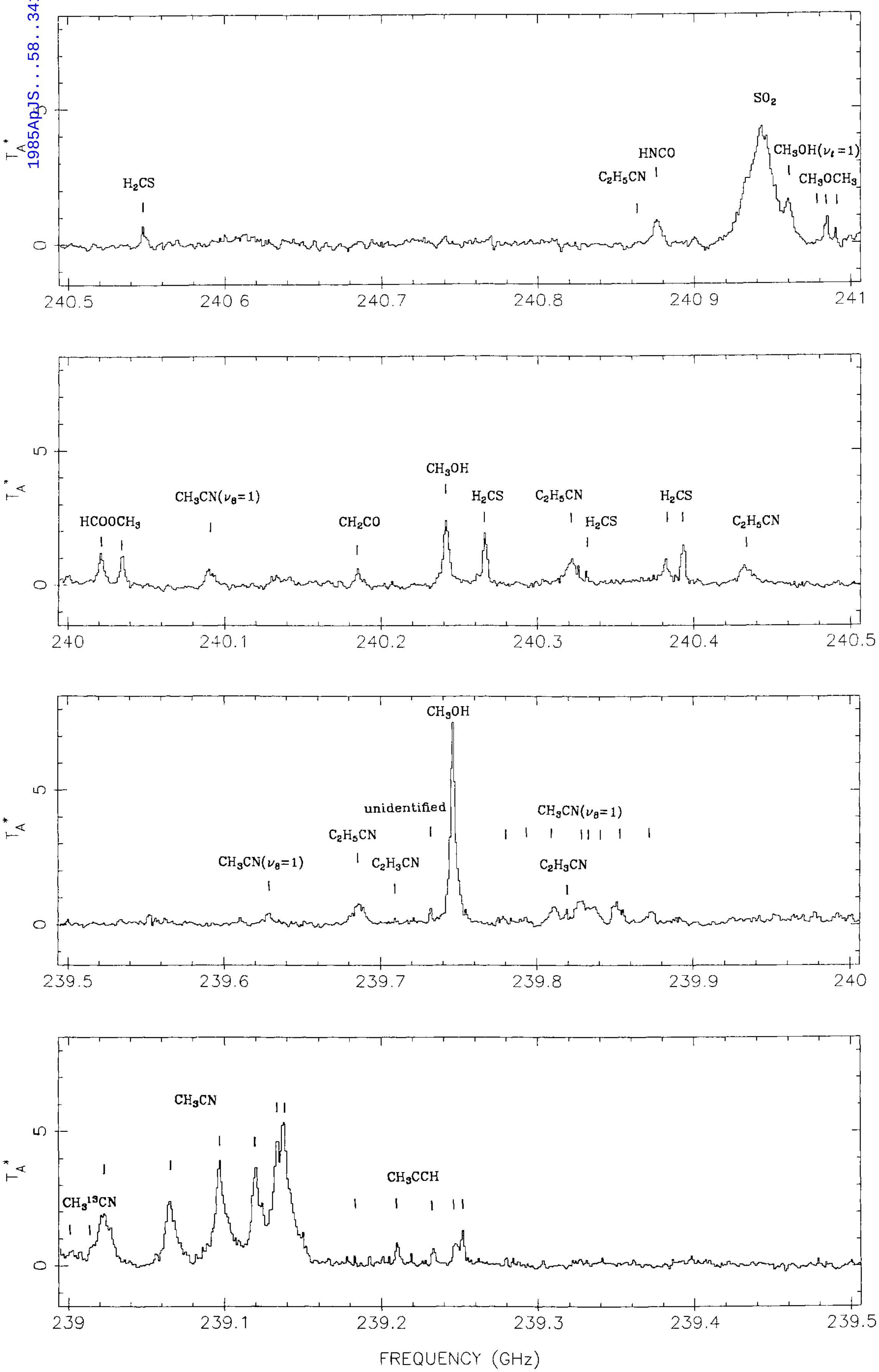

FIG. 1—*Continued*

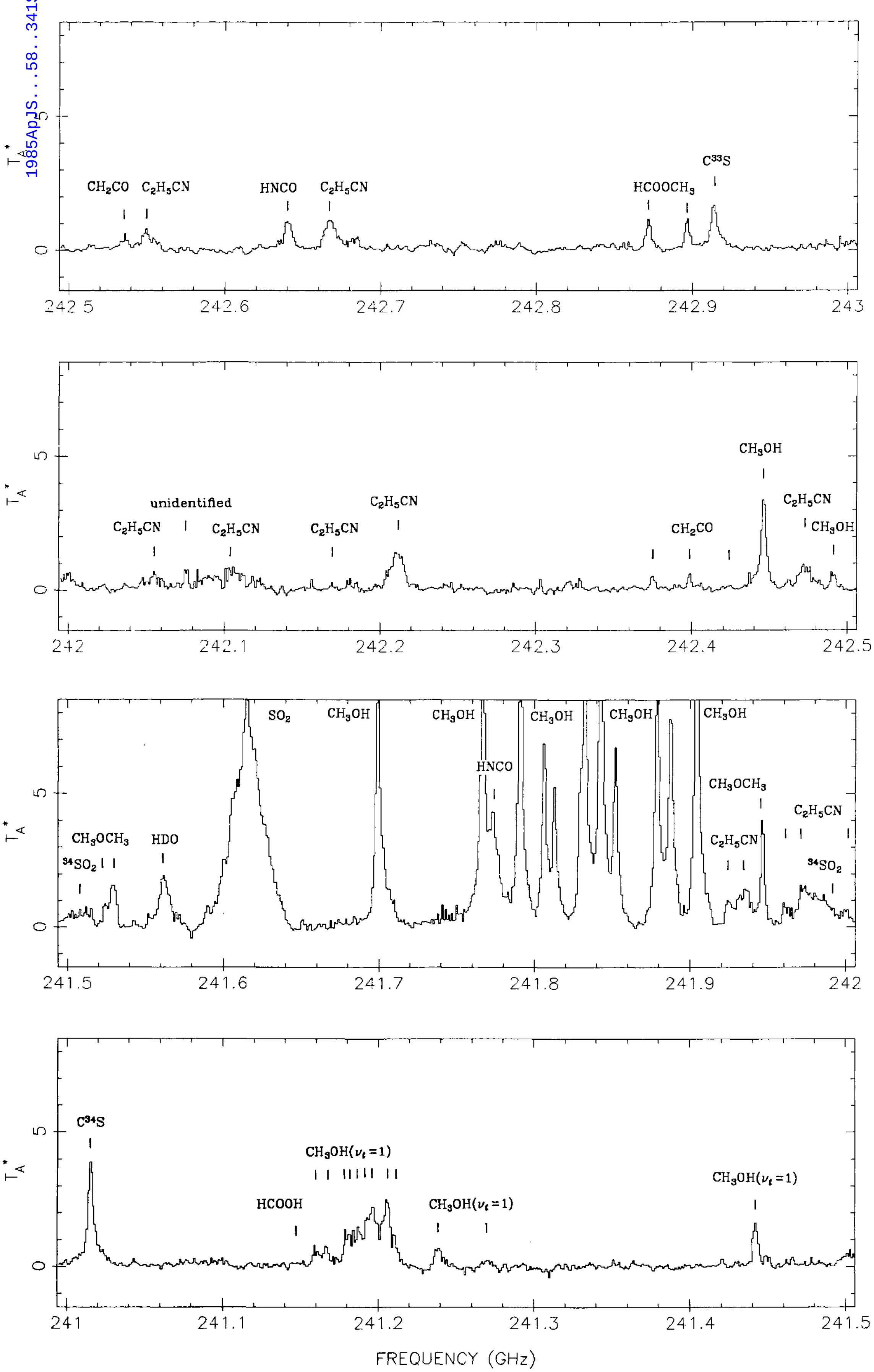

FIG. 1—*Continued*

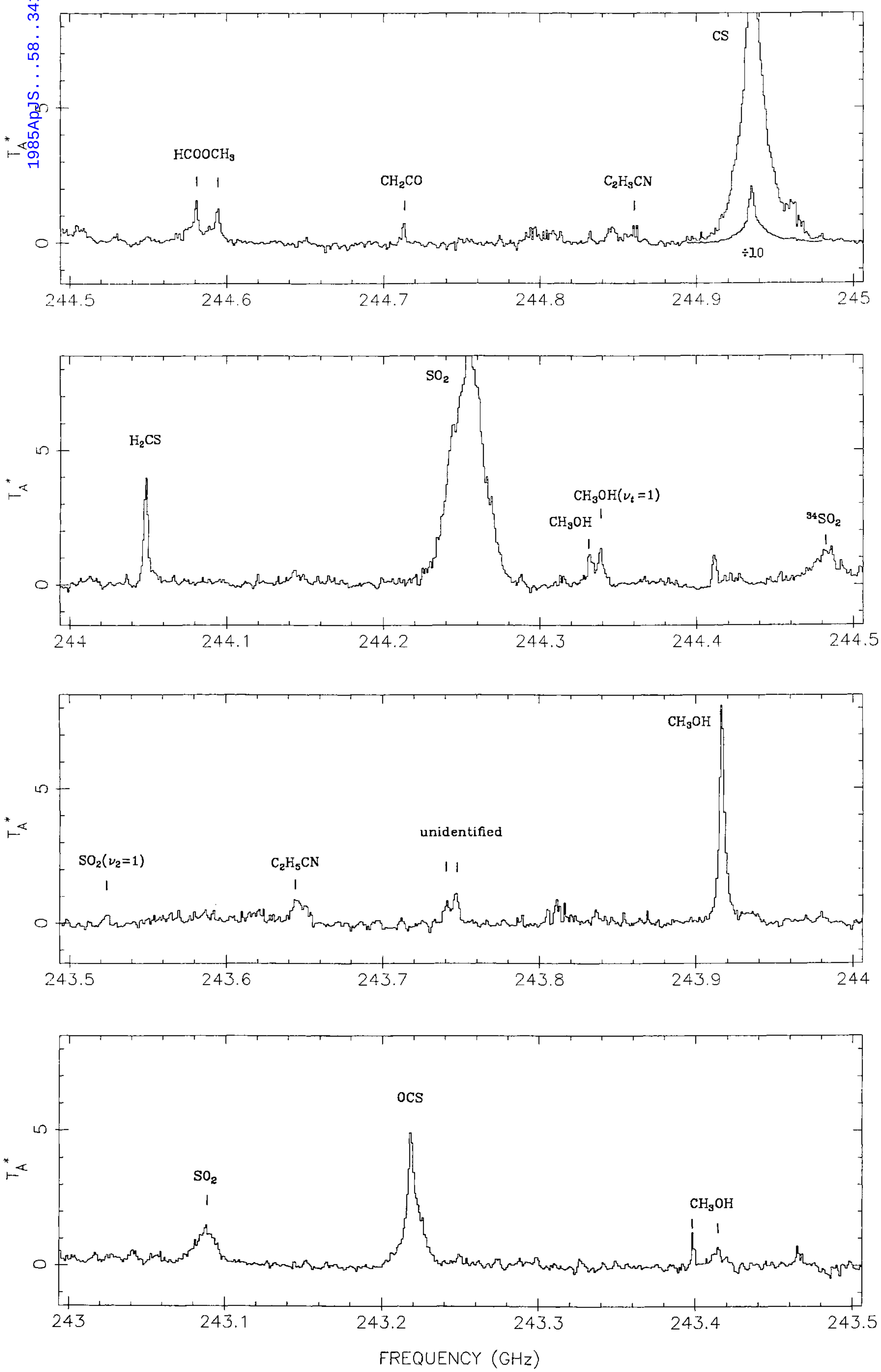

FIG. 1—*Continued*

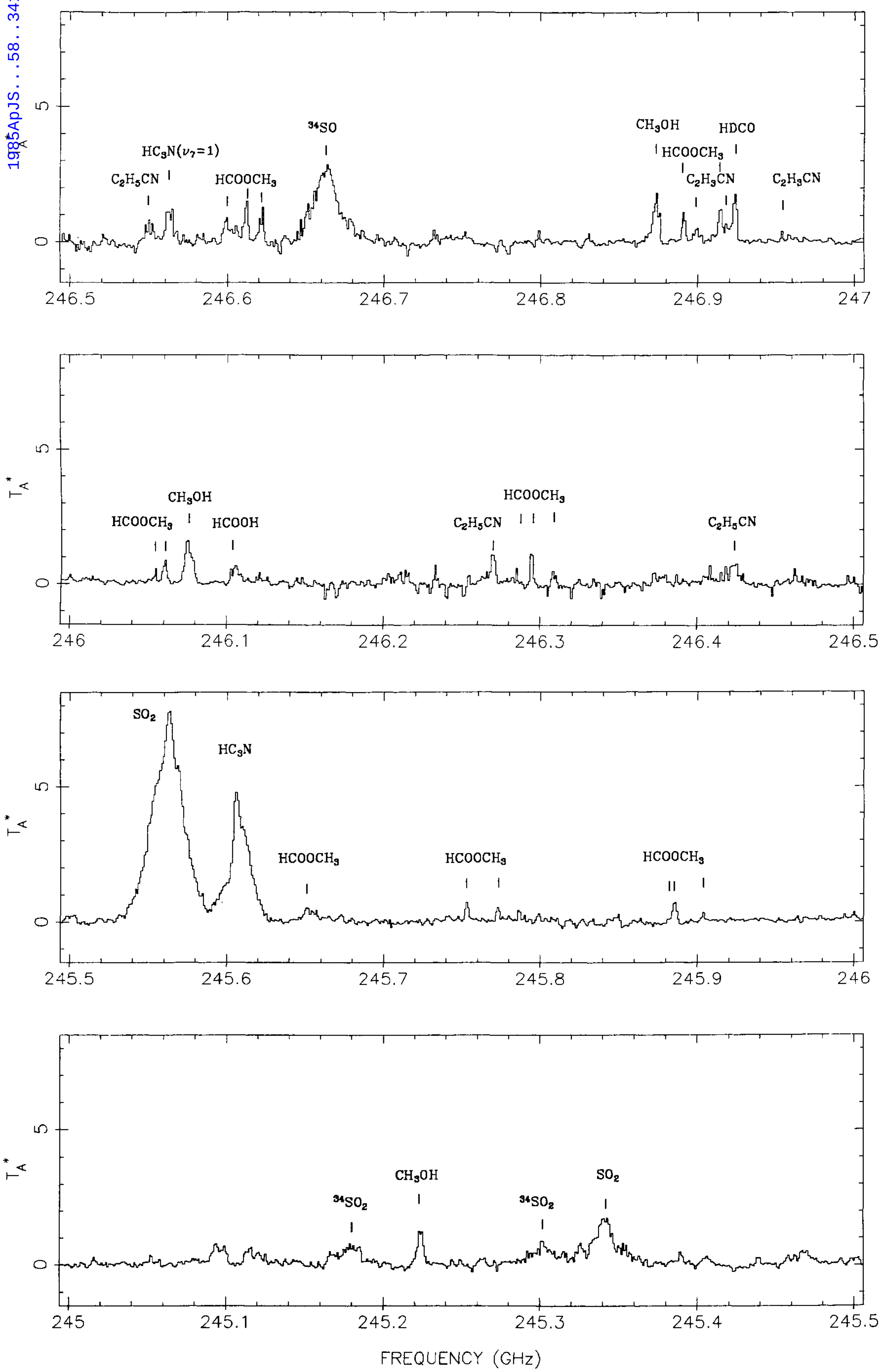

FIG. 1—*Continued*

TABLE 1

TRANSITIONS DETECTED FROM 215 TO 247 GHz

Frequency (MHz)	Species	Frequency (MHz)	Species	Frequency (MHz)	Species	Frequency (MHz)	Species
215041	C_2H_5CN	220399	^{13}CO	223119	$HCOOCH_3$	227028	$HCOOCH_3$
215059	C_2H_5CN	220476	CH_3CN	223125	$HCOOCH_3$	227032	$^{34}SO_2$
215088	C_2H_5CN	220539	CH_3CN	223135	$HCOOCH_3$	227095	unidentified
215109	C_2H_5CN	220561	C_2H_3CN	223163	$HCOOCH_3$	227419	HC_3N
215119	C_2H_5CN	220585	HNCO	223202	CH_3OCH_3	227562	$HCOOCH_3$
215127	C_2H_5CN	220594	CH_3CN	223385	C_2H_5CN	227781	C_2H_5CN
215173	C_2H_5CN	220621	$CH_3{}^{13}CN$	223434	SO_2	227815	unidentified
215221	SO	220634	$CH_3{}^{13}CN$	223554	C_2H_5CN	227898	C_2H_3CN
215302	$CH_3OH(\nu_t=1)$	220641	CH_3CN	223650	CH_3CHO	227907	C_2H_3CN
215401	C_2H_5CN	220661	C_2H_5CN	223661	CH_3CHO	227919	C_2H_3CN
215428	C_2H_5CN	220679	CH_3CN	223884	SO_2	227963	C_2H_3CN
215620	C_2H_5CN	220709	CH_3CN	223916	HCOOH	227977	$HC_3N(\nu_7=1)$
215840	^{34}SO	220730	CH_3CN	223934	C_2H_5CN	228091	C_2H_3CN
215886	unidentified	220743	CH_3CN	224002	C_2H_3CN	228105	C_2H_3CN
215986	C_2H_5CN	220747	CH_3CN	224018	C_2H_3CN	228303	$HC_3N(\nu_7=1)$
216000	$^{34}SO_2$	220812	$HCOOCH_3$	224023	$HCOOCH_3$	228483	C_2H_5CN
216077	C_2H_5CN	220815	$HCOOCH_3$	224028	C_2H_5CN	228544	HCOOH
216110	$HCOOCH_3$	220889	$HCOOCH_3$	224046	C_2H_3CN	228629	$HCOOCH_3$
216116	$HCOOCH_3$	220926	$HCOOCH_3$	224086	C_2H_5CN	228651	$HCOOCH_3$
216211	$HCOOCH_3$	220978	$HCOOCH_3$	224132	C_2H_5CN	228798	C_2H_5CN
216217	$HCOOCH_3$	221048	$HCOOCH_3$	224186	C_2H_5CN	228911	DNC
216569	H_2CO	221066	$HCOOCH_3$	224207	C_2H_5CN	228979	CH_3OCH_3
216643	SO_2	221124	C_2H_3CN	224265	SO_2	228983	CH_3OCH_3
216710	H_2S	221141	$HCOOCH_3$	224313	$HCOOCH_3$	229087	C_2H_3CN
216830	$HCOOCH_3$	221158	$HCOOCH_3$	224327	CH_2CO, $HCOOCH_3$	229265	C_2H_5CN
216839	$HCOOCH_3$	221199	$CH_3CN(\nu_8=1)$	224420	C_2H_5CN	229348	SO_2
216937	C_2H_3CN	221252	$CH_3CN(\nu_8=1)$	224459	C_2H_5CN	229405	$HCOOCH_3$
216946	CH_3OH	221261	$HCOOCH_3$	224469	C_2H_5CN	229420	$HCOOCH_3$
216966	$HCOOCH_3$	221266	$HCOOCH_3$	224493	unidentified	229475	$HCOOCH_3$
217105	SiO	221281	$HCOOCH_3$	224583	$HCOOCH_3$	229505	$HCOOCH_3$
217239	DCN	221300	$CH_3CN(\nu_8=1)$	224609	$HCOOCH_3$	229590	unidentified
217300	unidentified	221312	$CH_3CN(\nu_8=1)$	224640	C_2H_5CN	229648	C_2H_3CN
217817	SiS ?	221338	$CH_3CN(\nu_8=1)$	224699	unidentified	229759	CH_3OH
217823	unidentified	221350	$CH_3CN(\nu_8=1)$	224714	$C^{17}O$	229858	$^{34}SO_2$
217830	^{33}SO	221368	$CH_3CN(\nu_8=1)$	224895	unidentified	229864	CH_3OH
217887	unidentified	221381	$CH_3CN(\nu_8=1)$	225154	SO_2	229939	CH_3OH
218199	$O^{13}CS$	221387	$CH_3CN(\nu_8=1)$	225236	C_2H_5CN	230027	CH_3OH
218222	H_2CO	221394	$CH_3CN(\nu_8=1)$	225413	$OC^{34}S$	230233	unidentified
218281	$HCOOCH_3$	221404	$CH_3CN(\nu_8=1)$	225513	HCOOH	230318	$O^{13}CS$
218298	$HCOOCH_3$	221425	$CH_3CN(\nu_8=1)$, $HCOOCH_3$	225599	CH_3OCH_3	230369	CH_3OH
218325	HC_3N	221433	$HCOOCH_3$	225609	$HCOOCH_3$	230468	CH_3OCH_3
218390	C_2H_5CN	221446	$HCOOCH_3$	225619	$HCOOCH_3$	230538	CO
218422	C_2H_3CN	221626	$CH_3CN(\nu_8=1)$	225625	unidentified	230738	C_2H_3CN
218440	CH_3OH	221650	$HCOOCH_3$	225698	H_2CO	231061	OCS
218452	C_2H_3CN	221660	$HCOOCH_3$	225897	HDO	231199	$HCOOCH_3$
218476	H_2CO	221671	$HCOOCH_3$	225929	$HCOOCH_3$	231221	^{13}CS
218574	C_2H_3CN	221675	$HCOOCH_3$	226257	C_2H_3CN	231239	$HCOOCH_3$
218585	C_2H_3CN	221736	$^{34}SO_2$	226300	SO_2	231281	CH_3OH
218615	C_2H_3CN	221766	C_2H_3CN	226333	CN	231312	C_2H_5CN
218760	H_2CO	221965	SO_2	226342	CN	231506	HCOOH
218861	$HC_3N(\nu_7=1)$	222099	CH_3CCH	226347	CH_3OCH_3	231854	C_2H_5CN
218903	OCS	222129	CH_3CCH	226360	CN	231901	H30α
218981	HNCO	222150	CH_3CCH	226384	unidentified	231952	C_2H_3CN
219174	$HC_3N(\nu_7=1)$	222154	C_2H_3CN	226436	unidentified	231967	$HCOOCH_3$
219276	SO_2	222163	CH_3CCH	226552	CH_3CHO	231988	CH_3OCH_3
219355	$^{34}SO_2$	222167	CH_3CCH	226593	CH_3CHO	231990	C_2H_5CN
219401	C_2H_3CN	222177	unidentified	226617	CN	232163	unidentified
219464	C_2H_5CN	222198	CH_2CO	226634	CN, $HCOOCH_3$	232216	$^{13}CH_3CN$
219506	C_2H_5CN	222229	CH_2CO	226660	CN	232230	$^{13}CH_3CN$
219547	HNCO	222239	CH_3OCH_3	226664	CN	232234	$^{13}CH_3CN$
219560	$C^{18}O$	222248	CH_3OCH_3	226679	CN	232419	CH_3OH
219657	HNCO	222255	CH_3OCH_3	226713	$HCOOCH_3$	232784	CH_3OH
219734	HNCO	222259	unidentified	226719	$HCOOCH_3$	232790	C_2H_5CN
219737	HNCO	222314	CH_2CO	226773	$HCOOCH_3$	232945	CH_3OH
219798	HNCO	222422	$HCOOCH_3$	226779	$HCOOCH_3$	232965	C_2H_5CN
219909	$H_2{}^{13}CO$	222427	CH_3OCH_3	226857	$HCOOCH_3$	232976	C_2H_5CN
219949	SO	222435	CH_3OCH_3	226862	$HCOOCH_3$	233000	C_2H_5CN
220038	HCOOH	222439	$HCOOCH_3$	226875	CN	233041	C_2H_5CN
220079	CH_3OH	222707	C_2H_5CN	226887	CN	233069	C_2H_5CN
220167	$HCOOCH_3$	222723	unidentified	226892	CN	233089	C_2H_5CN
220178	CH_2CO	222918	C_2H_5CN	226905	CN	233145	C_2H_5CN
220190	$HCOOCH_3$	223038	$HCOOCH_3$	227020	$HCOOCH_3$	233207	C_2H_5CN

TABLE 1—*Continued*

Frequency (MHz)	Species	Frequency (MHz)	Species	Frequency (MHz)	Species	Frequency (MHz)	Species
233227	$HCOOCH_3$	236810	$HCOOCH_3$	240021	$HCOOCH_3$	242425	CH_2CO
233310	$HCOOCH_3$	236936	CH_3OH	240035	$HCOOCH_3$	242446	CH_3OH
233395	$HCOOCH_3$	236977	unidentified	240090	$CH_3CN(\nu_8=1)$	242470	C_2H_5CN
233443	C_2H_5CN	237049	CH_3OCH_3	240186	CH_2CO	242490	CH_3OH
233498	C_2H_5CN	237069	SO_2	240242	CH_3OH	242536	CH_2CO
233507	$HCOOCH_3$	237093	$HC_3N(\nu_7=1)$	240266	H_2CS	242547	C_2H_5CN
233524	C_2H_5CN, $HCOOCH_3$	237131	unidentified	240319	C_2H_5CN	242640	$HNCO$
233628	$HCOOCH_3$	237170	C_2H_5CN	240331	H_2CS	242665	C_2H_5CN
233650	$HCOOCH_3$	237267	$HCOOCH_3$	240381	H_2CS	242872	$HCOOCH_3$
233655	$HCOOCH_3$, C_2H_5CN	237273	$OC^{34}S$	240393	H_2CS	242896	$HCOOCH_3$
233671	$HCOOCH_3$	237298	$HCOOCH_3$	240429	C_2H_5CN	242914	$C^{33}S$
233754	$HCOOCH_3$	237308	$HCOOCH_3$	240548	H_2CS	243088	SO_2
233778	$HCOOCH_3$	237315	$HCOOCH_3$	240861	C_2H_5CN	243218	OCS
233796	CH_3OH	237345	$HCOOCH_3$	240876	$HNCO$	243398	CH_3OH
233845	$HCOOCH_3$	237350	$HCOOCH_3$	240943	SO_2	243413	CH_3OH
233854	$HCOOCH_3$	237405	C_2H_5CN, C_2H_3CN	240961	$CH_3OH(\nu_t=1)$	243523	$SO_2(\nu_2=1)$
233867	$HCOOCH_3$	237432	$HC_3N(\nu_7=1)$	240978	CH_3OCH_3	243643	C_2H_5CN
234011	$HCOOCH_3$, $^{13}CH_3OH$	237456	C_2H_3CN	240984	CH_3OCH_3	243740	unidentified
234112	$HCOOCH_3$	237484	C_2H_3CN	240990	CH_3OCH_3	243747	unidentified
234125	$HCOOCH_3$	237591	C_2H_3CN	241016	$C^{34}S$	243916	CH_3OH
234135	$HCOOCH_3$	237621	CH_3OCH_3	241146	$HCOOH$	244048	H_2CS
234187	SO_2	237712	C_2H_3CN	241159	$CH_3OH(\nu_t=1)$	244254	SO_2
234291	unidentified	237808	$HCOOCH_3$	241167	$CH_3OH(\nu_t=1)$	244331	CH_3OH
234329	$HCOOCH_3$	237830	$HCOOCH_3$	241179	$CH_3OH(\nu_t=1)$	244338	$CH_3OH(\nu_t=1)$
234422	SO_2, C_2H_5CN	237852	C_2H_5CN	241184	$CH_3OH(\nu_t=1)$	244482	$^{34}SO_2$
234486	$HCOOCH_3$	237983	$^{13}CH_3OH$	241187	$CH_3OH(\nu_t=1)$	244580	$HCOOCH_3$
234502	$HCOOCH_3$	238017	unidentified	241193	$CH_3OH(\nu_t=1)$	244594	$HCOOCH_3$
234509	$HCOOCH_3$	238156	$HCOOCH_3$	241197	$CH_3OH(\nu_t=1)$	244712	CH_2CO
234683	CH_3OH	238190	$HCOOCH_3$	241205	$CH_3OH(\nu_t=1)$	244857	C_2H_3CN
234698	CH_3OH	238727	C_2H_3CN	241211	$CH_3OH(\nu_t=1)$	244936	CS
234739	$HCOOCH_3$	238766	CH_3CN	241238	$CH_3OH(\nu_t=1)$	245179	$^{34}SO_2$
234936	PN ?	238796	C_2H_3CN	241268	$CH_3OH(\nu_t=1)$	245223	CH_3OH
235030	$HCOOCH_3$	238844	CH_3CN	241441	$CH_3OH(\nu_t=1)$	245302	$^{34}SO_2$
235047	$HCOOCH_3$	238913	CH_3CN	241509	$^{34}SO_2$	245339	SO_2
235051	$HCOOCH_3$	238927	$HCOOCH_3$	241524	CH_3OCH_3	245563	SO_2
235152	SO_2	238972	CH_3CN	241530	CH_3OCH_3	245606	HC_3N
235261	unidentified	238993	SO_2	241562	HDO	245651	$HCOOCH_3$
235564	C_2H_3CN	239001	$CH_3{}^{13}CN$	241616	SO_2	245752	$HCOOCH_3$
235845	$HCOOCH_3$	239015	$CH_3{}^{13}CN$	241700	CH_3OH	245772	$HCOOCH_3$
235866	$HCOOCH_3$	239023	CH_3CN	241767	CH_3OH	245883	$HCOOCH_3$
235881	$^{13}CH_3OH$	239064	CH_3CN	241774	$HNCO$	245885	$HCOOCH_3$
235887	$HCOOCH_3$	239097	CH_3CN	241791	CH_3OH	245904	$HCOOCH_3$
235928	$^{34}SO_2$	239120	CH_3CN	241807	CH_3OH	246055	$HCOOCH_3$
235932	$HCOOCH_3$	239133	CH_3CN	241813	CH_3OH	246061	$HCOOCH_3$
235938	$^{13}CH_3OH$	239138	CH_3CN	241831	CH_3OH	246075	CH_3OH
235952	$^{34}SO_2$	239179	CH_3CCH	241843	CH_3OH	246106	$HCOOH$
235960	$^{13}CH_3OH$	239211	CH_3CCH	241852	CH_3OH	246269	C_2H_5CN
235971	$^{13}CH_3OH$	239234	CH_3CCH	241879	CH_3OH	246285	$HCOOCH_3$
235997	$^{13}CH_3OH$	239248	CH_3CCH	241888	CH_3OH	246295	$HCOOCH_3$
236006	$^{13}CH_3OH$	239252	CH_3CCH	241904	CH_3OH	246308	$HCOOCH_3$
236008	$^{13}CH_3OH$	239627	$CH_3CN(\nu_8=1)$	241923	C_2H_5CN	246422	C_2H_5CN
236017	$^{13}CH_3OH$	239683	C_2H_5CN	241933	C_2H_5CN	246549	C_2H_5CN
236041	$^{13}CH_3OH$	239708	C_2H_3CN	241947	CH_3OCH_3	246561	$HC_3N(\nu_7=1)$
236050	$^{13}CH_3OH$	239732	unidentified	241959	C_2H_5CN	246600	$HCOOCH_3$
236062	$^{13}CH_3OH$	239746	CH_3OH	241970	C_2H_5CN	246613	$HCOOCH_3$
236217	SO_2	239777	$CH_3CN(\nu_8=1)$	241986	$^{34}SO_2$	246623	$HCOOCH_3$
236356	$HCOOCH_3$	239792	$CH_3CN(\nu_8=1)$	241997	C_2H_5CN	246663	^{34}SO
236366	$HCOOCH_3$	239809	$CH_3CN(\nu_8=1)$	242048	C_2H_5CN	246673	CH_3OH
236513	HC_3N	239816	C_2H_3CN	242077	unidentified	246891	$HCOOCH_3$
236717	$HCOOH$	239825	$CH_3CN(\nu_8=1)$	242102	C_2H_5CN	246897	C_2H_3CN
236726	H_2CS	239830	$CH_3CN(\nu_8=1)$	242167	C_2H_5CN	246915	$HCOOCH_3$
236744	$HCOOCH_3$	239836	$CH_3CN(\nu_8=1)$	242209	C_2H_5CN	246918	C_2H_3CN
236760	$HCOOCH_3$	239850	$CH_3CN(\nu_8=1)$	242376	CH_2CO	246925	$HDCO$
236801	$HCOOCH_3$	239872	$CH_3CN(\nu_8=1)$	242399	CH_2CO	246952	C_2H_3CN

A tabulation of the lines detected, presented in frequency order, is contained in Table 1. Listed are the appropriate rest frequencies and the molecules to which the emission is assigned. Further information on the exact line frequencies, the quantum numbers of the transitions, and the strengths of the astronomical emission is contained in the following sections on the individual molecules.

V. DISCUSSION OF INDIVIDUAL SPECIES

a) CO, CS, SiO, SiS, *and* SO

Many of the strongest individual lines in the spectrum are from diatomic molecules of the most abundant elements. Carbon monoxide (CO) provides the strongest line in the spectrum, its $J = 2$–1 transition at 230538 MHz. The species CS and SiO are isoelectronic with CO, yet have qualitatively different characteristics because of the very different abundances and dipole moments of these forms.

Emission from carbon monoxide (CO) and its isotopic forms is described in Table 2. The $J = 2$–1 line of the principal isotopic form, $^{12}C^{16}O$, is dominated by plateau emission. The full width to zero intensity of the line is approximately 150 MHz (200 km s^{-1}). The high-velocity wings of the line are particularly strong in these observations because of the small 0'.5 beamwidth which emphasizes emission from the compact plateau source. The ^{13}CO line is also extremely strong but with less pronounced wings. The variation in the $^{12}CO/^{13}CO$ intensity ratio across the line profile indicates that the transition in ^{12}CO is quite optically thick at line center but becomes optically thin at velocities of approximately ± 25 km s^{-1} relative to the line center. The intensities of the rarer isotopic forms $C^{18}O$ and $C^{17}O$ are consistent with optically thin emission at the velocity of the ambient molecular cloud ($v_{LSR} \approx 8.5$ km s^{-1}). Emission from $^{12}C^{16}O$ in the first vibrationally excited state was looked for but not detected.

CS is detected through its intense $J = 5$–4 line at 244936 MHz. This line also has a line shape with a strong plateau component, as expected due to the known concentration of sulfur-containing molecules in the plateau source. Several rarer isotopic forms are detected in ratios indicating that the parent line is optically thick and the isotopic lines optically thin. The isotopic lines, seen at $v_{LSR} = 8.4$ km s^{-1} with 7.3 km s^{-1} width, are dominated by the spike component, although the $C^{34}S$ line clearly shows broad plateau-type wings.

TABLE 2

TRANSITIONS OF CO, CS, SiO, AND SiS

Species	ν (MHz)	J	T_a^* (peak) (K)	$\int T_a^* dv$ (K km s^{-1})	Notes
CO	230538.0	2–1	111.	2242.	
^{13}CO	220398.7		37.6	319.	
$C^{18}O$	219560.3		5.7	39.4	
$C^{17}O$	224714.4		1.5	6.7	
CO($\nu = 1$)	228439.2		nd	...	
CS...........	244935.6	5–4	21.1	291.	
^{13}CS	231220.8		2.5	16.0	
$C^{34}S$	241016.2		3.9	33.5	
$C^{33}S$	242913.7		1.5	11.0	
CS($\nu = 1$)	243160.8		nd	...	
SiO	217104.9	5–4	8.1	278.	
SiO($\nu = 1$) ...	215596.0		nd	...	
SiS	217817.3	12–11	0.5?	4.5?	a
	235961.1	13–12	...	...	b

[a]Unusual v_{LSR}.
[b]Lost under $^{13}CH_3OH$ 235960.

Silicon monoxide (SiO) is detected through a single line of the dominant isotopic species. Again, the line shape is very broad (34.7 km s^{-1}), as is characteristic of the plateau source.

Silicon sulfide (SiS) has been reported in Orion A by Dickinson and Rodriguez-Kuiper (1981). Their detection of the $J = 6$–5 line gave an LSR velocity of 14 km s^{-1}, rather different from the 5–9 km s^{-1} range of most molecular components of Orion. Two transitions of SiS fall within the range of this survey. The $J = 13$–12 line at 235961 MHz falls in a band of $^{13}CH_3OH$ lines and is inaccessible. The $J = 12$–11 line at 217817 MHz is in a clear region. There is no line evident at "normal" velocities, ~ 8 km s^{-1}. There is, however, an otherwise unidentified line which could be interpreted as SiS at $v_{LSR} \approx 14$ km s^{-1}. Similarly, though, there is an even stronger line on the other side of the expected position which could be SiS at $v_{LSR} \approx 2$ km s^{-1}. In principle either or both of these velocities could be right, since such velocities are clearly present in Orion. However, it is hard to see why SiS should have such a different velocity structure from all the other molecules present. The 14 km s^{-1} velocity is perhaps more likely, since it is in coincidence with the previously reported detection. However, the detection of SiS at all in Orion still seems rather tentative.

Sulfur monoxide (SO) has a more complicated spectrum due to the presence of electronic angular momentum. The lines detected are listed in Table 3. There is a pair of strong lines from SO seen in the spectrum. Several other transitions in this frequency range are not detectable here because of their reduced line strengths. Two lines of ^{34}SO and one of ^{33}SO are also seen, but there is no clear detection of $S^{18}O$. All the lines detected exhibit the broad (average width 25.1 km s^{-1}) plateau lineshape often seen in sulfur-containing molecules.

b) CN

Emission from CN is seen in the $N=2-1$ spin multiplet centered near 227 GHz. The spin splitting, which is of the order of a few hundred megahertz, is further split by hyperfine structure. Emission from OMC-1 in this band was previously studied by Wootten *et al.* (1982). The current results are listed in Table 4, where the frequencies are taken from Skatrud *et al.* (1983). The results are consistent with those of Wootten *et al.*, showing central velocities of $v_{LSR}=9$ km s^{-1}, widths of 4 km s^{-1}, and a peak antenna temperature in the blended 226875 MHz transition of 9.1 K. The relative strengths of the hyperfine components show that the emission is just beginning to saturate in the strongest components ($\tau = 1.4 \pm 0.1$ at 226875 MHz), indicating a CN column density of around 1.5×10^{16} cm^{-2}.

c) PO *and* PN

Phosphorus-containing compounds have not been seen in the interstellar medium. Recent laboratory studies have shown that two of the most likely forms are the diatomics PO and PN (Thorne *et al.* 1984). Transition frequencies for the PO radical have been calculated (Pickett, private communication) based on the measurements of Kawaguchi, Saito, and Hirota (1983). Although four lines are predicted to fall in this frequency region, as shown in Table 5, there is no good evidence for emission at any of the expected frequencies. An upper limit of roughly 2×10^{14} cm^{-2} can be deduced from these data.

TABLE 3

Transitions of SO

Species	ν (MHz)	N_J	T_a^* (K)	$\int T_a^* dv$ (K km s^{-1})	Notes
SO	215220.6	5_5-4_4	20.0	562.	
	219949.4	6_5-5_4	24.7	680.	
	236452.3	1_2-2_1	0.4?	...	
^{34}SO ...	215839.9	6_5-5_4	3.9	93.9	
	246663.4	5_6-4_5	2.9	65.4	
^{33}SO ...	217830.	6_5-5_4	0.9	21.2	a
$S^{18}O$ ...	232265.9	5_6-4_5	0.3?	...	
	239128.5	6_6-5_5	...	...	b
	243039.3	7_6-6_5	0.4?	...	

[a] Blend of hyperfine components.
[b] Lost under CH_3CN 239120 and 239133.

TABLE 4

Transitions of CN

ν (MHz)	N, J, F	T_a^* (K)	$\int T_a^* dv$ (K km s^{-1})	Notes
226287.4	2,3/2,1/2–1,3/2,1/2	...	...	a
226298.9	2,3/2,1/2–1,3/2,3/2	...	...	a
226303.0	2,3/2,3/2–1,3/2,1/2	...	...	a
226314.6	2,3/2,3/2–1,3/2,3/2	...	...	a
226332.5	2,3/2,3/2–1,3/2,5/2	0.3	1.1	
226341.9	2,3/2,5/2–1,3/2,3/2	0.3	1.3	
226359.9	2,3/2,5/2–1,3/2,5/2	1.2	4.2	
226616.5	2,3/2,1/2–1,1/2,3/2	0.2	1.1	
226632.2	2,3/2,3/2–1,1/2,3/2	1.4	7.8	
226659.5	2,3/2,5/2–1,1/2,3/2	4.3	15.4	
226663.7	2,3/2,1/2–1,1/2,1/2	1.5	9.4	
226679.3	2,3/2,3/2–1,1/2,1/2	1.9	7.2	
226874.2	2,5/2,5/2–1,3/2,3/2 }			
226874.8	2,5/2,7/2–1,3/2,5/2 }	9.1	51.6	
226875.9	2,5/2,3/2–1,3/2,1/2 }			
226887.4	2,5/2,3/2–1,3/2,3/2	1.4	7.5	
226892.2	2,5/2,5/2–1,3/2,5/2	1.7	6.9	
226905.4	2,5/2,3/2–1,3/2,5/2	0.2	0.5	

[a] Lost under SO_2 226300.

TABLE 5

TRANSITIONS OF PO AND PN

Species	ν (MHz)	J, F	T_a^* (K)	$\int T_a^* dv$ (K km s^{-1})
PO......	239948.9	11/2,6–9/2,5 *e*	nd	...
	239958.1	11/2,5–9/2,4 *e*	nd	...
	240141.0	11/2,6–9/2,5 *f*	nd	...
	240152.5	11/2,5–9/2,4 *f*	nd	...
PN......	234935.7	5–4	0.4	1.5

TABLE 6

TRANSITIONS OF OCS

Species	ν (MHz)	J	T_a^* (K)	$\int T_a^* dv$ (K km s^{-1})
OCS......	218903.4	18–17	3.9	40.0
	231061.0	19–18	5.2	50.1
	243218.0	20–19	4.9	59.3
$OC^{34}S$ ...	225413.0	19–18	0.7	3.9
	237272.9	20–19	0.5	1.9
$O^{13}CS$ ...	218199.0	18–17	0.5	2.5
	230317.5	19–18	0.5	1.6
	242435.4	20–19	0.4?	...

PN has no electronic angular momentum and hence has a single rotational transition accessible. There is a weak line clearly present at the $J = 5$–4 frequency (Wyse, Manson, and Gordy 1972) which is not currently identified as due to any other molecular species. However, its identification as PN must await detection of some other transition in another frequency band, due to the number of weak lines of well-known species (e.g., CH_3OH) whose frequencies are currently unknown. If the line seen is due to PN, its v_{LSR} of 8 km s^{-1} and width of 4 km s^{-1} indicates it arises in the spike component. The column density of PN would be roughly 3×10^{12} cm^{-2} for an assumed rotational temperature of 100 K.

d) OCS

Carbonyl sulfide (OCS) is detected through emission in its $J = 18$–17, 19–18, and 20–19 lines. The results are presented in Table 6. The difference in line strengths is somewhat larger than expected, possibly indicating a calibration problem for the lowest frequency line. Line shapes clearly indicate the presence of both spike and plateau components. The isotope $OC^{34}S$ is detectable in our band through the $J = 19$–18 and 20–19 lines. The former is convincingly detected but at a level rather stronger than expected on the basis of an $OCS/OC^{34}S$ integrated intensity ratio of ~ 16 (Johansson *et al.* 1984). This is possibly the result of a coincidence with a currently unidentified line at this frequency. The $J = 20$–19 line of $OC^{34}S$ is marginally detected at about the level expected from the above ratio. $O^{13}CS$ may be detected, since there are indications of lines at the $J = 18$–17, 19–18, and 20–19 frequencies, although this would not be expected for an $OCS/O^{13}CS$ ratio of ~ 40.

e) DCN, DNC, *and* HC_3N

The $J = 3$–2 line of hydrogen cyanide (HCN) lies at higher frequency than the range presently searched. The only isotopic form accessible is deuterated hydrogen cyanide (DCN) and its isomer DNC. Both are detected here and the results shown in Table 7. DCN is the stronger line with a v_{LSR} of 9.3 km s^{-1} and a width of 7.9 km s^{-1}, not consistent with just spike component emission. DNC is weaker and seems to have just the narrower (8.7 km s^{-1} v_{LSR}, 3.3 km s^{-1} width) spike component.

Protonated hydrogen cyanide ($HCNH^+$) has not been seen in the interstellar medium. It is of considerable importance chemically as a precursor to both HCN and HNC. Molecular constants have recently been determined by Altman, Crofton, and Oka (1984), allowing prediction of the $J = 3$–2 frequency to a precision of about 10 MHz. This is sufficient to show that emission in this transition is not present in the spectrum of Orion A to a limit of $T_a^* < 0.2$ K (3 σ).

TABLE 7

TRANSITIONS OF DCN, DNC, $HCNH^+$, AND HC_3N

Species	ν (MHz)	J	T_a^* (K)	$\int T_a^* dv$ (K km s^{-1})
DCN	217238.5	3–2	2.9	21.8
DNC	228910.5	3–2	0.6	2.0
$HCNH^+$	222323.	3–2	nd	...
HC_3N	218324.8	24–23	4.0	62.1
	227419.0	25–24	3.5	41.5
	236512.8	26–25	3.5	53.6
	245606.4	27–26	4.8	81.6
$HC_3N(\nu_7)$	218860.6	24–23 1*e*	0.6	7.6
	219173.6	24–23 1*f*	0.6	9.2
	227977.1	25–24 1*e*	0.7	8.4
	228303.0	25–24 1*f*	0.8	10.8
	237093.2	26–25 1*e*	0.8	7.5
	237432.0	26–25 1*f*	0.7	9.9
	246208.9	27–26 1*e*	0.4?	...
	246560.7	27–26 1*f*	1.1	8.0

Cyanoacetylene (HC_3N) is seen in four of its pure rotational transitions, also shown in Table 7. The line shapes indicate the presence of spike, hot core, and plateau components. Isotopic forms ($H^{13}CCCN$, $HC^{13}CCN$, and $HCC^{13}CN$) were looked for but not convincingly detected. The ν_7 bending mode at 222 cm^{-1} is well excited under hot core conditions and the four pairs of vibrationally excited lines corresponding to the four ground-state lines are easily seen. Their average velocities ($v_{LSR} = 4.7$ km s^{-1}) and widths (11.3 km s^{-1}) confirm that this emission is from the hot core. More highly excited vibrational states (ν_6 and $2\nu_7$) are not detected.

Cyanodiacetylene (HC_5N) is not detected in any of the twelve pure rotational transitions which fall in this frequency band. This is consistent with the results of Johansson *et al.* (1984), who report a tentative detection of HC_5N with an integrated line strength of approximately 0.015 of the nearby HC_3N lines.

TABLE 8

TRANSITIONS OF DCO^+, N_2D^+, AND HCS^+

Species	ν (MHz)	J	T_a^* (K)	$\int T_a^* dv$ (K km s^{-1})	Notes
DCO^+ ...	216112.6	3–2	nd	...	a
N_2D^+	231321.8	3–2	nd	...	
HCS^+	213360.8	5–4	0.8	4.3	b

[a] Lost under $HCOOCH_3$ 216110 and 216116.

[b] This transition was seen in an incomplete set of measurements extending a few GHz below the nominal band discussed in this paper. It is included here since this was the only accessible transition of HCS^+. Due to the incomplete nature of this datum, its uncertainty is considerably greater than that of the rest of the data.

f) DCO^+, N_2D^+, *and* HCS^+

Two remaining deuterated linear molecules DCO^+ and N_2D^+ were looked for but not detected, as shown in Table 8. Also, HCS^+ was detected in observations just outside this frequency band. It exhibited a narrow line width of ~6 km s^{-1}, similar to the ^{13}CS line but without evidence of broad wings as seen in the ^{12}CS and OCS emission.

g) CH_3CN (CH_3NC) *and* CH_3CCH

The $J=13$–12 and $J=12$–11 bands of the symmetric top methyl cyanide (CH_3CN) were included within the spectral range covered here. The observed lines in the ground vibrational state are listed in Table 9. As discussed by Loren, Mundy, and Erickson (1981) and Loren and Mundy (1984), the low K lines ($K \leq 3$) are seen to be blends of hot core and spike components, with the higher K lines being almost entirely from the hot core. Excitation analysis of the two bands yields excitation temperatures of 285 K and 100 K for the hot core and spike methyl cyanide respectively. Column densities are approximately 2×10^{15} cm^{-2} and 2×10^{14} cm^{-2} for the two components.

Vibrationally-excited (ν_8) methyl cyanide, seen at lower J by Goldsmith *et al.* (1983), is seen here in a total of 23 lines. The lines detected are listed in Table 9. The average v_{LSR} of the ν_8 lines is 6.5 km s^{-1} and the average width is 8.0 km s^{-1}, corresponding to hot-core emission. The strengths of these lines are consistent with an extrapolation of the high K ground state lines at $T_{ex}=285$ K.

Isotopic methyl cyanide is detected in the form of $^{13}CH_3CN$. This species has a significantly different moment of inertia and its lines are well separated from the parent species. The bands of $CH_3{}^{13}CN$, on the other hand, are intermingled with the parent species and the evidence is less certain. The evidence for these isotopic forms is presented in Table 10.

Methyl isocyanide (CH_3NC) has not been convincingly detected in the interstellar medium. If its abundance were as great as is suggested by the DCN/DNC ratio, it should be easily detected here. The $J=13$–12 and $J=12$–11 bands fall within this frequency range. The former, unfortunately, is partly obstructed by lines of CH_3OH in the $J=5$–4 $\nu_t=1$ band. The $J=12$–11 band is relatively clear except for a competing line of $HCOOCH_3$. There is no clear evidence for emission from CH_3NC in the data, and its abundance relative to CH_3CN must be down by a factor of at least 10. This is in close agreement with the limit set by Irvine and Schloerb (1984) for TMC-1 based on 1.6 cm observations. It is at the low end of the range in the abundance of CH_3NC predicted by DeFrees, McLean, and Herbst (1984).

Methyl acetylene (CH_3CCH) is also seen in its $J=14$–13 and $J=13$–12 bands. This molecule shows spike component lineshapes ($v_{LSR}=8.8$ km s^{-1}, width $=4.5$ km s^{-1}) with a fairly low excitation temperature ($T_{ex}\approx60$ K). The lines detected are shown in Table 11. The inferred column density of this species is 10^{15} cm^{-2}.

h) CH_3OH

Emission from methanol (CH_3OH, Table 12) is concentrated in the strong $J=5$–4 *a*-type band between 239 and 244 GHz. However, higher and lower J *b*-type ($\Delta K=1$) transitions are sprinkled throughout the spectrum. Because of the large perturbations caused by the intermediate-height torsional barrier in methanol, frequency predictions are difficult and the available data often inadequate. Many of the high-J methanol lines were identified as such only long after they were first seen astronomically. Many more, currently unidentified, are probably due to methanol. The strong line at 232945 MHz was identified as due to methanol only after its laboratory detection in methanol vapor. The assignment of quantum numbers is still lacking.

The strongest of the methanol lines are clearly saturated. From the weaker lines a column density of around 5×10^{16} cm^{-2} can be derived. Excitation analysis reveals a trend toward higher rotational temperatures for the high-energy transitions, as noted by Hollis *et al.* (1983). The mean rotational temperature using all the lines is ~120 K, consistent with the narrow spike-component lineshapes and the v_{LSR} of 8 km s^{-1}. However, broad wings can clearly be seen on the strongest lines, indicating a methanol component in the hotter gas as well.

This warm, relatively quiescent gas is most easily seen in the torsionally excited *a*-type band at 241200 MHz. The lines are quite strong, indicating that the torsionally excited lines (as well as the high-energy ground-state lines) arise from optically thin and spatially compact material. Two torsionally excited *b*-type lines are also detected, but laboratory data at present are insufficient to accurately predict the frequencies of other such transitions in this frequency range. For the nonblended *a*-type and *b*-type lines the average v_{LSR} is 7.1 km s^{-1} and the average width is 5.5 km s^{-1}. This is clearly not emission from the hot core as seen in CH_3CN. Rather, it seems to be warm material in the compact ridge source (Oloffson 1984; Johansson *et al.* 1984).

Carbon-13 methanol ($^{13}CH_3OH$) has been seen in a total of 15 lines (Table 13). Its interpretation is discussed separately (Blake *et al.* 1984). The derived column density for $^{13}CH_3OH$ is $\sim1.3\times10^{15}$ cm^{-2}. Several lines previously identified as due to other chemical species are seen to be due instead to $^{13}CH_3OH$. In addition to the lines listed here, several *b*-type transitions of $^{13}CH_3OH$ should be strong enough to be detected. However, at the moment there are no adequate frequency predictions for these lines. Identification of the *b*-type $^{13}CH_3OH$ lines will await further laboratory and computational work.

TABLE 9

TRANSITIONS OF CH_3CN

ν (MHz)	J_K	T_a^* (K)	$\int T_a^* dv$ (K km s^{-1})	Notes
		CH_3CN		
220403.9	12_9-11_9	...	...	a
220475.8	12_8-11_8	0.5	2.9	
220539.3	12_7-11_7	0.9	5.3	
220594.4	12_6-11_6	1.9	22.9	
220641.1	12_5-11_5	2.1	20.1	
220679.3	12_4-11_4	2.5	19.0	
220709.0	12_3-11_3	4.9	48.2	
220730.3	12_2-11_2	4.4	60.3	
220743.0	12_1-11_1	~4.6	~67.	
220747.3	12_0-11_0	~5.3	~75.	
238766.1	13_9-12_9	0.4	2.4	
238843.9	13_8-12_8	0.6	5.8	
238912.7	13_7-12_7	0.7	5.4	
238972.4	13_6-12_6	1.7	15.6	
239022.9	13_5-12_5	1.7	23.4	
239064.3	13_4-12_4	2.3	28.0	
239096.5	13_3-12_3	3.9	46.1	
239119.5	13_2-12_2	3.7	35.3	
239133.3	13_1-12_1	~4.0	~40.	
239137.9	13_0-12_0	~4.5	~45.	
		$CH_3CN(\nu_8)$		
221199.0	12_1-11_1 (1)	0.7	10.9	b
221252.3	12_5-11_5 (−1)	0.3	1.8	
221265.1	12_7-11_7 (1)	...	...	c
221299.6	12_4-11_4 (−1)	0.2	0.8	
221311.9	12_6-11_6 (1)	0.2	1.9	
221338.0	12_3-11_3 (−1)	0.3	1.7	
221350.3	12_5-11_5 (1)	0.2	1.6	
221367.5	12_2-11_2 (−1)	0.6	6.2	
221380.6	12_4-11_4 (1)	0.6	4.1	
221387.3	12_1-11_1 (−1)	0.4	2.5	
221394.1	12_0-11_0 (1)	0.5	3.0	
221403.5	12_3-11_3 (1)	0.3	2.4	
221422.3	12_2-11_2 (1)	0.3	2.4	d
221626.0	12_1-11_1 (1)	0.4	2.9	
239627.2	13_1-12_1 (1)	0.4	3.5	
239684.6	13_5-12_5 (−1)	...	...	e
239699.3	13_7-12_7 (1)	nd	...	
239735.7	13_4-12_4 (−1)	...	...	f
239750.0	13_6-12_6 (1)	...	...	f
239777.2	13_3-12_3 (−1)	0.3	2.1	
239791.7	13_5-12_5 (1)	0.2	2.0	
239808.9	13_2-12_2 (−1)	0.6	6.4	
239824.8	13_4-12_4 (1)	0.8	8.2	
239830.0	13_1-12_1 (−1)	0.5	4.6	
239836.1	13_0-12_0 (1)	0.5	5.0	
239850.0	13_3-12_3 (1)	0.7	6.2	
239871.7	13_2-12_2 (1)	0.4	2.3	
240089.8	13_1-12_1 (1)	0.6	5.8	

[a] Lost under ^{13}CO 220399.
[b] Emission too broad to be entirely CH_3CN.
[c] Lost under $HCOOCH_3$ 221266.
[d] Blend with $HCOOCH_3$ 221425.
[e] Lost under C_2H_5CN 239683.
[f] Lost under CH_3OH 239746.

i) H_2CO, HDCO, H_2CS, HCOOH, *and* CH_3CHO

Formaldehyde (H_2CO) is a fairly light asymmetric top with a small handful of lines in this frequency band. The lines detected are shown in Table 14. Line shapes exhibit both narrow spike components and broad plateau emission, as discussed by Wootten, Loren, and Bally (1984). Line-strength differences for the few lines detected suggest an excitation temperature of ~100 K and an H_2CO column density of about 5×10^{15} cm^{-2}. Only two isotopic lines (one of $H_2{}^{13}CO$ and one of HDCO) are clearly detected.

Several lines of H_2CS are detected in the $J=7$–6 band. The lines are predominantly narrow ($v_{LSR}=7.5$ km s^{-1}, $\Delta v=4.3$ km s^{-1}) but with some evidence of broad wings. The

TABLE 10

TRANSITIONS OF $^{13}CH_3CN$ AND $CH_3{}^{13}CN$

Species	ν (MHz)	J_K	T_a^* (K)	$\int T_a^* dv$ (K km s^{-1})	Notes
$^{13}CH_3CN$	232194.6	13_3-12_3	0.7?	5.1?	a
	232216.4	13_2-12_2	0.5	4.0	
	232229.5	13_1-12_1	0.5	4.3	
	232233.9	13_0-12_0	0.6	4.7	
$CH_3{}^{13}CN$.......	220599.9	12_3-11_3	...	...	b
	220621.1	12_2-11_2	0.5	1.9	
	220633.8	12_1-11_1	0.5	2.2	c
	220638.0	12_0-11_0	...	...	d
	238978.3	13_3-12_3	...	...	e
	239001.2	13_2-12_2	0.3	1.3	
	239015.0	13_1-12_1	0.5	2.5	f
	239019.5	13_0-12_0	...	...	g

[a] Too strong relative to $K = 0$, 1, and 2; possible blend with unidentified line.
[b] Lost under CH_3CN 220594.
[c] Blended with CH_3CN 220641.
[d] Lost under CH_3CN 220641.
[e] Lost under CH_3CN 238972.
[f] Blended with CH_3CN 239023.
[g] Lost under CH_3CN 239023.

TABLE 11

TRANSITIONS OF CH_3CCH

ν (MHz)	J_K	T_a^* (K)	$\int T_a^* dv$ (K km s^{-1})
222099.2	13_4-12_4	0.2	0.9
222128.8	13_3-12_3	0.9	4.0
222150.0	13_2-12_2	1.1	6.0
222162.7	13_1-12_1	1.5	5.8
222167.0	13_0-12_0	1.6	8.6
239179.3	14_4-13_4	0.3	1.0
239211.2	14_3-13_3	0.9	4.3
239234.0	14_2-13_2	0.7	2.7
239247.7	14_1-13_1	0.9	4.0
239252.3	14_0-13_0	1.2	6.3

excitation temperature is similar to that of H_2CO, and the column density is roughly 10^{15} cm^{-2}. No isotopic forms of H_2CS are seen.

Formic acid (HCOOH) was not detected in Orion in the Onsala line survey (Johansson *et al.* 1984). Its absence was rather surprising, given the great abundance of the more complicated but structurally similar molecule methyl formate (§ V*m*). It seems to be detected here in small amounts, based on the data in Table 15. The average velocity for the emission is $v_{LSR} = 7.8$ km s^{-1} and the width is 4.6 km s^{-1}. Assuming $T_{ex} \approx 90$ K as for methyl formate and chemically similar species, the derived column density is $\sim 10^{14}$ cm^{-2}, which is near the limit set by the Onsala observations.

Acetaldehyde (CH_3CHO) is possibly seen here, although the evidence is not completely convincing. As shown in Table 16, there are weak bumps present at all the expected frequencies except at 216581 MHz. As discussed by Blake *et al.* (1984), the line at 236049 MHz is due primarily to $^{13}CH_3OH$. Acetaldehyde, if present, is certainly not very abundant.

j) CH_2CO *and* HNCO

The tentative detection of ketene (CH_2CO) in OMC-1 reported by Johansson *et al.* (1984) is definitely confirmed here with the detection of a total of 10 lines (Table 17). Line shapes are narrow (4.9 km s^{-1}) with a $v_{LSR} = 8.0$ km s^{-1} and an excitation temperature of around 120 K suggested, consistent with spike component emission. The column density is estimated to be 5×10^{14} cm^{-2}.

Isocyanic acid (HNCO) has been seen in Orion by Goldsmith *et al.* (1982) and Johansson *et al.* (1984). The broad emission component reported by Goldsmith *et al.* is easily seen here, particularly in the strong 219798 MHz line (Table 18). The average $v_{LSR} = 7.1$ km s^{-1} and the average width is 7.2 km s^{-1}. Excitation temperatures of ~ 120 K and column densities of 5×10^{14} cm^{-2} are consistent with the data reported here.

k) HDO *and* H_2S

Deuterated water (HDO) is detected through two of its

TABLE 12

TRANSITIONS OF CH_3OH

Species	ν (MHz)	J_K		T_a^* (K)	$\int T_a^* dv$ (K km s^{-1})	notes
CH_3OH....	216945.6	4_2-5_1	E	3.0	17.8	
	218440.0	4_2-3_1	E	8.4	41.1	
	220078.6	7_1-8_0	E	6.1	35.2	
	220401.0	$10_{-5}-11_{-4}$	E	...	...	a
	229758.7	$8_{-1}-7_0$	E	11.0	56.9	
	229864.2	19_5-20_4	A+	0.4	2.3	
	229939.2	19_5-20_4	A-	0.5	1.9	
	230027.1	$3_{-2}-4_{-1}$	E	5.1	24.2	
	230368.7	22_4-21_5	E	0.2	1.4	
	231281.1	10_2-9_3	A-	3.0	18.6	
	232418.6	10_2-9_3	A+	3.9	27.1	
	232783.5	18_3-17_4	A+	1.4	9.0	
	232945.	unassigned		3.0	20.0	b
	233795.8	18_3-17_4	A-	1.0	4.3	
	234683.2	4_2-5_1	A-	2.6	14.6	
	234698.4	$5_{-4}-6_{-3}$	E	1.2	4.6	
	236936.1	14_1-13_2	A-	2.3	15.8	
	239746.3	5_1-4_1	A+	7.4	42.9	
	240241.5	5_3-6_2	E	2.3	15.1	
	241700.2	5_0-4_0	E	9.3	~62.	
	241767.2	$5_{-1}-4_{-1}$	E	10.4	~85.	
	241791.4	5_0-4_0	A	10.7	61.4	
	241806.5	5_4-4_4	A±	6.5	41.3	
	241813.3	$5_{-4}-4_{-4}$	E	5.0	22.8	
	241829.6	5_4-4_4	E	} 9.6	68.3	
	241833.0	5_3-4_3	A±			
	241842.3	5_2-4_2	A-	} 10.3	84.6	
	241843.6	5_3-4_3	E			
	241852.4	$5_{-3}-4_{-3}$	E	6.6	28.6	
	241879.1	5_1-4_1	E	9.2	54.8	
	241887.7	5_2-4_2	A+	7.8	49.4	
	241904.4	$5_{-2}-4_{-2}$	E	} 11.8	69.8	
	241904.5	5_2-4_2	E			
	242446.2	$13_{-2}-14_{-1}$	E	3.3	22.5	
	242490.3	$24_{-3}-24_{+2}$	A	0.7	4.0	
	243397.5	18_6-19_5	A+	1.6	5.1	
	243412.6	$23_{-3}-23_{+2}$	A	0.9	4.0	
	243915.8	5_1-4_1	A-	8.1	50.5	
	244330.5	$22_{-3}-22_{+2}$	A	1.1	6.0	
	245223.0	$21_{-3}-21_{+2}$	A	1.3	7.6	
	246074.7	$20_{-3}-20_{+2}$	A	1.6	11.3	
	246873.3	$19_{-3}-19_{+2}$	A	1.8	10.7	
$CH_3OH(\nu_t=1)$	215302.2	6_1-7_2	A+	1.3	6.0	
	240960.6	5_1-4_1	A+	0.9	4.9	
	241159.1	5_4-4_4	E	0.7	5.0	
	241166.5	5_3-4_3	E	0.8	4.4	
	241178.4	5_4-4_4	A±	} 1.3	7.9	
	241179.9	$5_{-3}-4_{-3}$	E			
	241184.1	$5_{-4}-4_{-4}$	E	1.1	6.2	
	241187.4	$5_{-2}-4_{-2}$	E	1.4	8.4	
	241192.8	5_2-4_2	A+	1.9	11.4	
	241196.4	5_2-4_2	A-	} 2.1	12.4	
	241198.3	5_3-4_3	A±			
	241203.7	5_1-4_1	E	} 2.8	16.8	
	241206.0	5_0-4_0	E			
	241210.7	5_2-4_2	E	1.2	7.3	
	241238.2	$5_{-1}-4_{-1}$	E	0.7	4.4	
	241267.9	5_0-4_0	A	0.4	3.7	
	241441.2	5_1-4_1	A-	1.5	9.3	
	244338.0	9_1-8_0	E	1.2	8.4	

[a] Lost under ^{13}CO 220399.

[b] Rest frequency from laboratory measurement.

TABLE 13

TRANSITIONS OF $^{13}CH_3OH$

ν (MHz)	J_K	T_a^* (K)	$\int T_a^* dv$ (K km s^{-1})	Notes
234011.6	$5_1-4_1\ A+$	0.8	3.1	a
235881.2	$5_0-4_0\ E$	0.6	2.5	
235938.2	$5_{-1}-4_{-1}\ E$	0.7	2.8	b
235960.4	$5_0-4_0\ A\pm$	0.7	2.9	c
235971.1	$5_4-4_4\ A\pm$	0.3	1.0	
235978.6	$5_{-4}-4_{-4}\ E$	0.1?	...	
235994.4	$5_4-4_4\ E$ }	0.7	3.3	
235997.2	$5_3-4_3\ A\pm$ }			
236006.1	$5_3-4_3\ E$	0.4	1.4	
236008.4	$5_2-4_2\ A-$	0.7	2.7	
236016.6	$5_{-3}-4_{-3}\ E$	0.4	1.5	
236041.4	$5_1-4_1\ E$	0.6	2.3	
236049.5	$5_2-4_2\ A+$	0.4	1.7	
236062.0	$5_{-2}-4_{-2}\ E$ }	0.9	3.8	
236062.9	$5_2-4_2\ E$ }			
237983.4	$5_1-4_1\ A-$	0.8	3.5	

[a]Blend with $HCOOCH_3$ 234012.
[b]Blend with $^{34}SO_2$ 235928.
[c]Blend with $^{34}SO_2$ 235952.

TABLE 14

TRANSITIONS OF H_2CO AND H_2CS

Species	ν (MHz)	$J_{K_pK_o}$	T_a^* (K)	$\int T_a^* dv$ (K km s^{-1})	Notes
H_2CO	216568.6	$9_{1,8}-9_{1,9}$	1.3	6.1	
	218222.2	$3_{0,3}-2_{0,2}$	12.7	114.4	
	218475.6	$3_{2,2}-2_{2,1}$	6.2	40.9	
	218760.1	$3_{2,1}-2_{2,0}$	6.9	51.0	
	225697.8	$3_{1,2}-2_{1,1}$	21.6	181.5	
	227583.5	$17_{2,15}-17_{2,16}$	nd	...	
$H_2{}^{13}CO$	219908.5	$3_{1,2}-2_{1,1}$	2.7	10.3	
HDCO	227668.1	$1_{1,1}-0_{0,0}$	nd	...	
	228866.3	$6_{1,5}-6_{0,6}$	nd	...	
	246924.7	$4_{1,4}-3_{1,3}$	1.8	7.5	
H_2CS	236726.3	$7_{1,7}-6_{1,6}$	2.7	13.2	
	240261.4	$7_{5,3}-6_{5,2}$ }	0.2?	...	
		$7_{5,2}-6_{5,1}$ }			
	240266.2	$7_{0,7}-6_{0,6}$	1.9	9.1	
	240331.4	$7_{4,4}-6_{4,3}$ }	0.5	1.9	
		$7_{4,3}-6_{4,2}$ }			
	240381.3	$7_{2,6}-6_{2,5}$	0.7	3.1	
	240392.3	$7_{3,5}-6_{3,4}$ }	1.4	6.5	
	240393.0	$7_{3,4}-6_{3,3}$ }			
	240548.3	$7_{2,5}-6_{2,4}$	0.7	4.1	
	244047.8	$7_{1,6}-6_{1,5}$	3.9	17.1	
$H_2C^{34}S$	232778.5	$7_{1,7}-6_{1,6}$	nd	...	
	236198.8	$7_{0,7}-6_{0,6}$	...	...	a
	239858.5	$7_{1,6}-6_{1,5}$	nd	...	

[a]Lost under SO_2 236217.

low-lying transitions, as listed in Table 19. A third higher J transition falls in a very crowded region of the spectrum and may be present; however, it is difficult to separate its contribution from that of C_2H_5CN and $^{34}SO_2$. The HDO lines have predominantly hot-core line shapes ($v_{LSR} = 6.8$ km s^{-1}, $\Delta v = 11.5$ km s^{-1}), as best illustrated by the 225897 MHz line. Assuming a rotational temperature of 150 K, typical of many hot-core species, a column density of 4×10^{15} cm^{-2} is derived.

A single line of H_2S was detected. Its line shape seems to indicate both hot-core emission and the broader plateau-source component typical of sulfur-containing molecules.

l) SO_2

The molecule SO_2 dominates the appearance of the millimeter-wave spectrum of Orion. Because of its asymmetric geometry, it has a rich spectrum of lines which are typically very strong because of the large abundance and high dipole moment of the molecule. Emission from SO_2 accounts for approximately 28% of the total line flux from Orion. The detected lines of SO_2 and $^{34}SO_2$ are shown in Tables 20 and 21 respectively. The lines have predominantly plateau line shapes with average widths of 23.7 km s^{-1} for SO_2 and 17.0 km s^{-1} for $^{34}SO_2$. The strongest lines are clearly saturated. The weaker lines are fitted with an excitation temperature of about 95 K and inferred column density of 5×10^{16} cm^{-2}, similar to the values given by Schloerb *et al.* (1983).

Vibrationally excited SO_2 is probably detected on the basis of the $14_{0,14}-13_{1,13}$ line at 243522.6 MHz, as shown in Table 20. This is the strongest expected vibrationally excited line and has a lower state energy of ~ 580 cm^{-1} (Goldsmith *et al.* 1983). Its intensity is consistent with an extrapolation of the higher energy ground-state lines (e.g., $21_{7,15}-22_{6,16}$) at T_{rot} = 150 K, the temperature suggested by Schloerb *et al.* for their highest energy lines. The vibrationally excited emission has a (poorly determined) v_{LSR} of 6.5 km s^{-1} and a width of ~ 6 km s^{-1}. This is somewhat suggestive of hot-core emission but not conclusive, due to the weakness of the feature. It is interesting to note that the tentatively detected $27_{8,20}-28_{7,21}$ ground state line at 343 cm^{-1} also suggests hot-core emission ($v_{LSR} \approx 4.8$ km s^{-1}, $\Delta v \approx 8$ km s^{-1}).

TABLE 15

TRANSITIONS OF HCOOH

ν (MHz)	$J_{K_pK_o}$	T_a^* (K)	$\int T_a^* dv$ (K km s^{-1})	Notes
215407.8......	$10_{1,10}-9_{1,9}$	...	...	a
220038.0......	$10_{0,10}-9_{0,9}$	0.3	1.2	
223915.6......	$10_{2,9}-9_{2,8}$	0.3	1.0	
225237.8......	$10_{3,8}-9_{3,7}$	...	...	b
225512.5......	$10_{3,7}-9_{3,6}$	0.4	2.0	
228544.1......	$10_{2,8}-9_{2,7}$	0.4	1.2	
231505.6......	$10_{1,9}-9_{1,8}$	0.8	2.4	
236717.2......	$11_{1,11}-10_{1,10}$	0.4	1.5	
241146.2......	$11_{0,11}-10_{0,10}$	0.2	1.6	
246106.0......	$11_{2,10}-10_{2,9}$	0.6	4.8	c

[a] Lost under C_2H_5CN 215401.
[b] Lost under C_2H_5CN 225236.
[c] Too strong, possible blend with unidentified line.

TABLE 16

TRANSITIONS OF CH_3CHO

ν (MHz)	$J_{K_pK_o}$	T_a^* (K)	$\int T_a^* dv$ (K km s^{-1})	Notes
216580.6......	$11_{1,10}-10_{1,9}$ *E*	nd	...	
216630.0......	$11_{1,10}-10_{1,9}$ *A*	...	...	a
223650.3......	$12_{1,12}-11_{1,11}$ *E*	0.2	0.8	
223660.8......	$12_{1,12}-11_{1,11}$ *A*	0.3	2.4	
226551.5......	$12_{0,12}-11_{0,11}$ *E*	0.3	2.1	
226592.8......	$12_{0,12}-11_{0,11}$ *A*	0.2	1.0	
235997.0......	$12_{1,11}-11_{1,10}$ *E*	...	...	b
236049.1......	$12_{1,11}-11_{1,10}$ *A*	...	...	c

[a] Lost under SO_2 216643.
[b] Lost under $^{13}CH_3OH$ 235997.
[c] Lost under $^{13}CH_3OH$ 236050.

TABLE 17

TRANSITIONS OF CH_2CO

ν (MHz)	$J_{K_pK_o}$	T_a^* (K)	$\int T_a^* dv$ (K km s^{-1})	Notes
220177.5......	$11_{1,11}-10_{1,10}$	1.0	3.7	
222197.7......	$11_{0,11}-10_{0,10}$	0.6	3.7	
222228.6......	$11_{2,10}-10_{2,9}$	0.2	0.6	
222314.4......	$11_{2,9}-10_{2,8}$	0.2	0.6	
224327.2......	$11_{1,10}-10_{1,9}$	...	...	a
240185.8......	$12_{1,12}-11_{1,11}$	0.5	5.0	
242375.8......	$12_{0,12}-11_{0,11}$	0.5	2.7	
242398.7...... 242399.2......	$12_{3,10}-11_{3,9}$ $12_{3,9}-11_{3,8}$ }	0.6	2.9	
242424.7......	$12_{2,11}-11_{2,10}$	0.2	1.5	
242536.2......	$12_{2,10}-11_{2,9}$	0.4	2.5	
244712.2......	$12_{1,11}-11_{1,10}$	0.8	3.0	

[a] Blend with $HCOOCH_3$ 224328.

TABLE 18

TRANSITIONS OF HNCO

ν (MHz)	$J_{K_pK_o}$	T_a^* (K)	$\int T_a^* dv$ (K km s^{-1})	Notes
218981.0......	$10_{1,10}-9_{1,9}$	1.0	9.8	
219547.1......	$10_{4,7}-9_{4,6}$ $10_{4,6}-9_{4,5}$ }	0.4	2.3	
219656.8......	$10_{3,8}-9_{3,7}$ $10_{3,7}-9_{3,6}$ }	0.4	1.9	
219733.8......	$10_{2,9}-9_{2,8}$	0.6	3.5	
219737.2......	$10_{2,8}-9_{2,7}$	0.8	4.4	
219798.3......	$10_{0,10}-9_{0,9}$	2.9	35.3	
220584.8......	$10_{1,9}-9_{1,8}$	1.3	9.0	
240875.7......	$11_{1,11}-10_{1,10}$	0.9	7.0	
241619.3......	$11_{3,9}-10_{3,8}$	...	...	a
241619.4......	$11_{3,8}-10_{3,7}$	...	...	a
241703.8......	$11_{2,10}-10_{2,9}$	...	...	b
241708.3......	$11_{2,9}-10_{2,8}$	...	...	b
241774.0......	$11_{0,11}-10_{0,10}$	3.1	23.8	c
242639.7......	$11_{1,10}-10_{1,9}$	1.1	8.8	

[a] Lost under SO_2 241616.
[b] Blend with CH_3OH 241700.
[c] Blend with CH_3OH 241767.

TABLE 19

TRANSITIONS OF HDO AND H_2S

Species	ν (MHz)	$J_{K_pK_o}$	T_a^* (K)	$\int T_a^* dv$ (K km s^{-1})	Notes
HDO ...	225896.7	$3_{1,2}-2_{2,1}$	2.3	25.0	
	241561.5	$2_{1,1}-2_{1,2}$	1.9	23.1	
	241973.5	$7_{3,4}-6_{4,3}$	?	...	a
H_2S	216710.4	$2_{2,0}-2_{1,1}$	3.5	31.3	

[a] Blend with C_2H_5CN 241970 and $^{34}SO_2$ 241986.

TABLE 20

TRANSITIONS OF SO_2

Species	ν (MHz)	$J_{K_pK_o}$	T_a^* (K)	$\int T_a^* dv$ (K km s^{-1})	Notes
SO_2	216643.3	$22_{2,20}-22_{1,21}$	4.6	105.	
	219276.0	$22_{7,15}-23_{6,18}$	0.3?	...	
	221965.2	$11_{1,11}-10_{0,10}$	13.9	348.	
	223434.4	$27_{8,20}-28_{7,21}$	0.3?	...	
	223883.6	$6_{4,2}-7_{3,5}$	1.4	27.1	
	224264.9	$20_{2,18}-19_{3,17}$	2.6	60.8	
	225153.7	$13_{2,12}-13_{1,13}$	6.3	159.	
	226300.0	$14_{3,11}-14_{2,12}$	5.8	143.	
	229347.7	$11_{5,7}-12_{4,8}$	1.9	40.1	
	234187.1	$28_{3,25}-28_{2,26}$	1.6	36.1	
	234421.7	$16_{6,10}-17_{5,13}$	1.5	36.8	a
	235151.7	$4_{2,2}-3_{1,3}$	5.6	145.	
	236216.7	$16_{1,15}-15_{2,14}$	5.3	131.	
	237068.8	$12_{3,9}-12_{2,10}$	5.9	171.	
	238992.6	$21_{7,15}-22_{6,16}$	0.4	6.8	
	240942.8	$18_{1,17}-18_{0,18}$	4.3	111.	
	241615.8	$5_{2,4}-4_{1,3}$	8.9	225.	
	243087.7	$5_{4,2}-6_{3,3}$	1.4	24.5	
	243245.4	$26_{8,18}-27_{7,21}$	nd	...	
	244254.2	$14_{0,14}-13_{1,13}$	9.9	271.	
	245339.4	$26_{3,23}-25_{4,22}$	1.7	31.0	
	245563.4	$10_{3,7}-10_{2,8}$	7.8	220.	
$SO_2(\nu_2=1)$	243522.6	$14_{0,14}-13_{1,13}$	0.5	3.2	

[a] Blend with C_2H_5CN 234,424.

TABLE 21

TRANSITIONS OF $^{34}SO_2$

ν (MHz)	$J_{K_pK_o}$	T_a^* (K)	$\int T_a^* dv$ (K km s^{-1})	Notes
215999.8......	$14_{3,11}-14_{2,12}$	0.7	12.0	
219355.1......	$11_{1,11}-10_{0,10}$	1.3	24.0	
221735.7......	$13_{2,12}-13_{1,13}$	1.0	17.5	
227031.9......	$12_{3,9}-12_{2,10}$	0.7	14.6	a
229857.7......	$4_{2,2}-3_{1,3}$	1.1	21.0	
230933.5......	$5_{4,2}-6_{3,3}$	nd	...	
235927.5......	$5_{2,4}-4_{1,3}$	0.6	14.8	
235952.0......	$10_{3,7}-10_{2,8}$	0.7	19.1	
241509.0......	$16_{1,15}-15_{2,14}$	0.9	13.8	
241985.5......	$8_{3,5}-8_{2,6}$	1.4	29.2	
243935.9......	$18_{1,17}-18_{0,18}$	0.4?	...	
244481.5......	$14_{0,14}-13_{1,13}$	1.4	19.5	
245178.7......	$15_{2,14}-15_{1,15}$	0.8	14.2	
245302.3......	$6_{3,3}-6_{2,4}$	0.9	14.3	
246686.2......	$4_{3,1}-4_{2,2}$	0.3?	...	

[a] Blend with $HCOOCH_3$ 227028.

m) $HCOOCH_3$

The largest number of lines in the spectrum produced by any one molecule are due to methyl formate ($HCOOCH_3$). The 130 lines detected here are listed in Table 22. Methyl formate is a heavy asymmetric rotor with hindered internal rotation of the methyl group. Plummer *et al.* (1984) have measured transitions for the *A* symmetry state and have obtained accurate line-frequency predictions from a model which does not explicitly take into account the internal rotation. The *E* symmetry state has also recently been investigated by Plummer *et al.* (1985), using a model incorporating the internal rotation. The predicted frequencies are used here. In addition, Plummer *et al.* (1985) have measured directly all strongly perturbed transitions in this frequency range to eliminate any uncertainties in the rest frequencies. Measured line intensities for methyl formate imply an excitation temperature of ~ 90 K and a column density of 3×10^{15} cm^{-2}. The v_{LSR} of 7.8 km s^{-1}, velocity widths of ~ 4.3 km s^{-1}, and low excitation temperature indicate that methyl formate is spike-component material.

TABLE 22

TRANSITIONS OF $HCOOCH_3$

ν (MHz)	$J_{K_pK_o}$		T_a^* (K)	$\int T_a^* dv$ (K km s^{-1})	notes
215972.0....	$19_{1,18}-18_{2,17}$	A	0.2 ?	...	
216109.7....	$19_{2,18}-18_{2,17}$	E	0.9	4.5	
216115.5....	$19_{2,18}-18_{2,17}$	A	1.1	5.8	
216210.9....	$19_{1,18}-18_{1,17}$	E	0.8	4.3	
216216.5....	$19_{1,18}-18_{1,17}$	A	0.9	4.3	
216360.0....	$19_{2,18}-18_{1,17}$	A	0.2 ?	...	
216830.1....	$18_{2,16}-17_{2,15}$	E	1.2	3.9	
216838.8....	$18_{2,16}-17_{2,15}$	A	1.1	3.8	
216964.8....	$20_{1,20}-19_{1,19}$	E			
216965.9....	$20_{1,20}-19_{1,19}$	A	2.0	12.5	
216966.2....	$20_{0,20}-19_{0,19}$	E			
216967.3....	$20_{0,20}-19_{0,19}$	A			
218281.0....	$17_{3,14}-16_{3,13}$	E	1.0	4.2	
218297.8....	$17_{3,14}-16_{3,13}$	A	1.2	4.3	
220166.6....	$17_{4,13}-16_{4,12}$	E	1.3	5.8	
220190.2....	$17_{4,13}-16_{4,12}$	A	1.3	7.2	
220811.6....	$18_{3,16}-17_{2,15}$	E	0.4	1.0	
220815.2....	$18_{3,16}-17_{2,15}$	A	0.4	2.5	
220889.0....	$18_{17,2}-17_{17,1}$	A	0.4	2.3	
	$18_{17,1}-17_{17,0}$	A			
220926.2....	$18_{16,3}-17_{16,2}$	A	0.5	2.1	
	$18_{16,2}-17_{16,1}$	A			
220977.8....	$18_{15,3}-17_{15,2}$	A	0.5	3.2	
	$18_{15,4}-17_{15,3}$	A			
221047.7....	$18_{14,4}-17_{14,3}$	A			
	$18_{14,5}-17_{14,4}$	A	0.5	4.5	
221050.0....	$18_{14,4}-17_{14,3}$	E			
221066.3....	$18_{14,5}-17_{14,4}$	E	0.3	2.0	
221141.0....	$18_{13,5}-17_{13,4}$	A			
	$18_{13,6}-17_{13,4}$	A	0.7	4.0	
	$18_{13,5}-17_{13,4}$	E			
221158.4....	$18_{13,6}-17_{13,5}$	E	0.2	0.8	
221260.9....	$18_{12,6}-17_{12,5}$	E	0.4	1.0	
221265.6....	$18_{12,6}-17_{12,5}$	A	0.6	2.3	
	$18_{12,7}-17_{12,6}$	A			
221280.8....	$18_{12,7}-17_{12,6}$	E	0.4	1.6	
221424.7....	$18_{11,7}-17_{11,6}$	E	0.8	4.4	a
221433.0....	$18_{11,7}-17_{11,6}$	A	0.9	3.8	
	$18_{11,8}-17_{11,7}$	A			
221445.5....	$18_{11,8}-17_{11,7}$	E	0.6	2.6	
221649.7....	$18_{10,8}-17_{10,7}$	E	0.5	1.9	
221660.4....	$18_{4,15}-17_{4,14}$	E			
221661.1....	$18_{10,8}-17_{10,7}$	A	1.5	6.3	
	$18_{10,9}-17_{10,8}$	A			
221670.5....	$18_{10,9}-17_{10,8}$	E	0.4	1.6	
221674.6....	$18_{4,15}-17_{4,14}$	A	0.8	4.3	
221979.3....	$18_{9,10}-17_{9,9}$	A	...	...	b
221979.4....	$18_{9,9}-17_{9,8}$	A	...	...	b
222421.6....	$18_{8,10}-17_{8,9}$	E	1.0	5.2	
222438.2....	$18_{8,10}-17_{8,9}$	A			
222440.3....	$18_{8,11}-17_{8,10}$	A	1.2	10.8	c
222441.9....	$18_{8,10}-17_{8,9}$	E			
223038.3....	$19_{2,17}-18_{3,16}$	E	0.3	0.8	
223051.7....	$19_{2,17}-18_{3,16}$	A	0.2 ?	...	
223119.2....	$18_{7,12}-17_{7,11}$	A	1.1	5.5	
223125.1....	$18_{7,12}-17_{7,11}$	E	1.0	5.4	
223134.9....	$18_{7,11}-17_{7,10}$	E	1.0	4.6	
223162.7....	$18_{7,11}-17_{7,10}$	A	0.8	2.7	
224021.4....	$18_{6,13}-17_{6,12}$	E	1.0	7.5	d
224024.1....	$18_{6,13}-17_{6,12}$	A			
224312.9....	$18_{5,14}-17_{5,13}$	E	0.8	2.9	
224328.3....	$18_{5,14}-17_{5,13}$	A	0.8	3.2	e
224583.0....	$18_{6,12}-17_{6,11}$	E	0.8	3.2	
224609.3....	$18_{6,12}-17_{6,11}$	A	0.8	2.8	
225608.7....	$19_{3,17}-18_{3,16}$	E	1.1	5.0	
225618.7....	$19_{3,17}-18_{3,16}$	A	1.3	6.3	
225928.6....	$6_{6,1}-5_{5,0}$	A	0.4	2.2	
	$6_{6,0}-5_{5,1}$	A			
226635.2....	$20_{1,19}-19_{2,18}$	A	...	...	f
226713.1....	$20_{2,19}-19_{2,18}$	E	0.9	2.6	
226718.7....	$20_{2,19}-19_{2,18}$	A	0.5	2.6	
226773.2....	$20_{1,19}-19_{1,18}$	E	0.9	3.7	
226778.7....	$20_{1,19}-19_{1,18}$	A	1.0	3.1	
226856.5....	$20_{2,19}-19_{1,18}$	E	0.5	2.0	
226862.2....	$20_{2,19}-19_{1,18}$	A	0.6	1.8	
227019.6....	$19_{2,17}-18_{2,16}$	E	1.0	4.2	
227028.0....	$19_{2,17}-18_{2,16}$	A	1.2	4.5	g
227561.1....	$21_{0,21}-20_{0,20}$	E			
227561.9....	$21_{1,21}-20_{1,20}$	E	2.1	13.0	
227562.0....	$21_{1,21}-20_{1,20}$	A			
227562.8....	$21_{0,21}-20_{0,20}$	A			
228629.1....	$18_{5,13}-17_{5,12}$	E	1.2	4.0	
228651.3....	$18_{5,13}-17_{5,12}$	A	1.2	5.5	
229404.9....	$18_{3,15}-17_{3,14}$	E	1.2	5.0	
229420.3....	$18_{3,15}-17_{3,14}$	A	1.3	4.4	
229474.6....	$20_{3,17}-19_{4,16}$	E	0.3	0.9	
229504.6....	$20_{3,17}-19_{4,16}$	A	0.3	1.5	
229590.0....	$19_{3,17}-18_{2,16}$	E	...	...	h
229595.0....	$19_{3,17}-18_{2,16}$	A	...	...	h
231199.3....	$21_{9,12}-21_{8,13}$	A	0.3	1.8	
231239.1....	$21_{9,13}-21_{8,14}$	A	0.4	2.8	
231960.2....	$20_{9,11}-20_{8,12}$	E	nd	...	
231966.9....	$20_{9,11}-20_{8,12}$	A	0.4	1.6	
233212.6....	$19_{4,16}-18_{4,15}$	E	...	...	i
233226.7....	$19_{4,16}-18_{4,15}$	A	1.1	4.8	
233310.0....	$19_{15,4}-18_{15,3}$	A	0.4	2.2	
	$19_{15,5}-18_{15,4}$	A			
233394.6....	$19_{14,5}-18_{14,4}$	A	0.4	3.3	
	$19_{14,6}-18_{14,5}$	A			
233505.0....	$19_{13,7}-18_{13,6}$	E	...	...	j
233506.6....	$19_{13,6}-18_{13,5}$	A	0.8	7.0	
	$19_{13,7}-18_{13,6}$	A			
233524.6....	$19_{13,6}-18_{13,5}$	E	0.4	3.0	k
233627.1....	$17_{9,8}-17_{8,9}$	A	0.4	7.1	
233628.4....	$17_{9,9}-17_{8,10}$	A			
233649.9....	$19_{12,7}-18_{12,6}$	E	0.5	3.1	
233655.3....	$19_{12,7}-18_{12,6}$	A	1.1	8.2	l
	$19_{12,8}-18_{12,7}$	A			
233671.0....	$19_{12,8}-18_{12,7}$	E	0.3	2.0	
233754.1....	$18_{4,14}-17_{4,13}$	E	0.8	4.5	
233777.5....	$18_{4,14}-17_{4,13}$	A	0.8	3.0	
233845.3....	$19_{11,8}-18_{11,7}$	E	0.5	3.1	
233854.2....	$19_{11,8}-18_{11,7}$	A	0.7	3.1	
	$19_{11,9}-18_{11,8}$	A			
233867.1....	$19_{11,9}-18_{11,8}$	E	0.4	1.6	
234011.3....	$16_{9,7}-16_{8,8}$	A	...	...	m
234011.8....	$16_{9,8}-16_{8,9}$	A	...	...	m
234112.3....	$19_{10,9}-18_{10,8}$	E	0.3	2.3	
234124.8....	$19_{10,9}-18_{10,8}$	A	0.6	2.9	
	$19_{10,10}-18_{10,9}$	A			
234134.6....	$19_{10,10}-18_{10,9}$	E	0.6	3.0	
234328.8....	$15_{9,6}-15_{8,7}$	A	0.3 ?	...	
234328.9....	$15_{9,7}-15_{8,8}$	A			
234486.4....	$19_{9,10}-18_{9,9}$	E	0.6	3.5	
234502.2....	$19_{9,11}-18_{9,10}$	A	1.1	6.5	
234502.4....	$19_{9,10}-18_{9,9}$	A			
234508.5....	$19_{9,11}-18_{9,10}$	E	0.6	3.7	
234739.0....	$20_{2,18}-19_{3,17}$	A	0.5	0.9	

TABLE 22—*Continued*

ν (MHz)	$J_{K_pK_o}$	T_a^* (K)	$\int T_a^* dv$ (K km s^{-1})	notes
235029.9....	$19_{8,11}-18_{8,10}$ E	1.2	2.4	
235043.2....	$19_{8,12}-18_{8,11}$ E	} 0.6	2.5	
235046.5....	$19_{8,12}-18_{8,11}$ A			
235051.4....	$19_{8,11}-18_{8,10}$ A	1.2	5.1	
235844.5....	$19_{7,13}-18_{7,12}$ A	0.5	2.1	
235865.9....	$19_{7,13}-18_{7,12}$ E	0.5	2.1	
235887.2....	$19_{7,12}-18_{7,11}$ E	0.5	2.0	
235932.3....	$19_{7,12}-18_{7,11}$ A	0.5	1.6	n
236355.9....	$20_{3,18}-19_{3,17}$ E	0.9	5.8	
236365.5....	$20_{3,18}-19_{3,17}$ A	0.7	3.9	
236743.7....	$19_{5,15}-18_{5,14}$ E	0.6	2.4	
236759.6....	$19_{5,15}-18_{5,14}$ A	0.6	2.6	
236800.5....	$19_{6,14}-18_{6,13}$ E	0.6	2.7	
236810.3....	$19_{6,14}-18_{6,13}$ A	0.8	2.8	
237266.9....	$21_{1,20}-20_{2,19}$ A	0.4	3.3	
237297.5....	$20_{2,18}-19_{2,17}$ E	0.8	3.5	
237306.0....	$20_{2,18}-19_{2,17}$ A	} 1.1	8.6	
237309.5....	$21_{2,20}-20_{2,19}$ E			
237315.1....	$21_{2,20}-20_{2,19}$ A	1.1	6.2	
237344.8....	$21_{1,20}-20_{1,19}$ E	0.8	2.6	
237350.4....	$21_{1,20}-20_{1,19}$ A	0.7	2.4	
237393.2....	$21_{2,20}-20_{1,19}$ E	0.1 ?	...	
237398.6....	$21_{2,20}-20_{1,19}$ A	0.2 ?	...	
237807.6....	$19_{6,13}-18_{6,12}$ E	0.5	2.3	
237829.8....	$19_{6,13}-18_{6,12}$ A	0.6	2.3	
238156.2....	$22_{1,22}-21_{1,21}$ E	} 2.7	21.1	
238156.6....	$22_{0,22}-21_{0,21}$ E			
238156.8....	$22_{1,22}-21_{1,21}$ A			
238157.3....	$22_{0,22}-21_{0,21}$ A			
238190.1....	$7_{6,2}-6_{5,1}$ A	} 0.2	1.7	
238190.2....	$7_{6,1}-6_{5,2}$ A			
238926.8....	$20_{3,18}-19_{2,17}$ E	0.3	0.9	
238932.5....	$20_{3,18}-19_{2,17}$ A	0.1 ?	...	
240021.4....	$19_{3,16}-18_{3,15}$ E	1.0	5.9	
240034.6....	$19_{3,16}-18_{3,15}$ A	1.1	4.9	
242872.2....	$19_{5,14}-18_{5,13}$ E	1.1	6.5	
242896.0....	$19_{5,14}-18_{5,13}$ A	1.1	6.1	
244580.7....	$20_{4,17}-19_{4,16}$ E	1.3	5.3	
244594.0....	$20_{4,17}-19_{4,16}$ A	1.1	5.4	
245137.9....	$21_{3,18}-20_{4,17}$ E	0.3 ?	...	
245165.8....	$21_{3,18}-20_{4,17}$ A	0.4 ?	...	
245651.1....	$20_{16,5}-19_{16,4}$ A	} 0.6	3.2	
	$20_{15,6}-19_{15,5}$ A			
245752.2....	$20_{14,6}-19_{14,5}$ A	} 0.7	2.3	
	$20_{14,7}-19_{14,6}$ A			
245754.3....	$20_{14,6}-19_{14,5}$ E			
245772.1....	$20_{14,7}-19_{14,6}$ E	0.5	1.8	
245883.2....	$20_{13,8}-19_{13,7}$ E	0.2	0.5	
245885.1....	$20_{13,7}-19_{13,6}$ A	} 0.8	3.3	
	$20_{13,8}-19_{13,7}$ A			
245903.5....	$20_{13,7}-19_{13,6}$ E	0.2	0.9	
246055.1....	$20_{12,9}-19_{12,8}$ E	0.5	1.0	
246060.8....	$20_{12,8}-19_{12,7}$ A	} 0.8	3.0	
	$20_{12,9}-19_{12,8}$ A			
246076.6....	$20_{12,8}-19_{12,7}$ E	...	...	o
246285.4....	$20_{11,9}-19_{11,8}$ E	0.4	1.5	
246295.1....	$20_{11,10}-19_{11,9}$ A	} 1.3	3.0	
	$20_{11,9}-19_{11,8}$ A			
246308.6....	$20_{11,10}-19_{11,9}$ E	0.4	2.0	
246600.2....	$20_{10,11}-19_{10,10}$ E	0.7	3.3	
246613.3....	$20_{10,11}-19_{10,10}$ A	} 1.1	4.8	
246613.4....	$20_{10,10}-19_{10,9}$ A			
246623.1....	$20_{10,10}-19_{10,9}$ E	0.8	3.7	
246891.1....	$19_{4,15}-18_{4,14}$ E	1.2	3.4	
246914.6....	$19_{4,15}-18_{4,14}$ A	1.2	5.5	

[a] Blend with $CH_3CN(\nu_8)$ 221422.
[b] Lost under SO_2 221965.
[c] Blend with CH_3OCH_3 222435.
[d] Blend with C_2H_5CN 224018.
[e] Blend with CH_2CO 224327.
[f] Blend with CN 226632.
[g] Blend with $^{34}SO_2$ 227032.
[h] Blend with unidentified line.
[i] Lost under C_2H_5CN 233207.
[j] Blend with C_2H_5CN 233498.
[k] Blend with C_2H_5CN 233524.
[l] Blend with C_2H_5CN 233654.
[m] Blend with $^{13}CH_3OH$ 234012.
[n] Blend with $^{34}SO_2$ 235928.
[o] Lost under CH_3OH 246075.

Lines in the first excited torsional state of methyl formate are in principle detectable due to the low energy (~100 cm^{-1}) of the torsional motion. Frequency predictions for such lines have not yet been made. However, there should be hundreds of such lines additionally present at about the noise level of the spectrum (~0.1 K).

n) CH_3OCH_3

Dimethyl ether (CH_3OCH_3) is detected on the basis of 14 rotational transitions, as listed in Table 23. The lines are narrow, with intrinsic widths of ~3 km s^{-1}, and are centered at $v_{LSR} \approx 8$ km s^{-1}, typical of the spike component of the molecular cloud. Each rotational transition is split by the hindered internal rotation of the two methyl groups into four components corresponding to the four allowed symmetry states. This splitting is generally resolved in the spectra, except for transitions with low values for the oblate rotor quantum number *K*. The variation in the observed line intensities yields an excitation temperature of 80 K and an inferred column density for CH_3OCH_3 of 3×10^{15} cm^{-2}.

o) C_2H_3CN *and* C_2H_5CN

Vinyl cyanide (C_2H_3CN) and ethyl cyanide (C_2H_5CN) are heavy asymmetric rotors which show emission from a large number of lines in this frequency band involving highly excited levels. Because of their large moments of inertia, values for the total angular momentum range generally from $J=23$ to $J=28$ for most of these lines. Typical upper-state energies for these levels are ~100–200 cm^{-1} above the ground state. The lines detected are listed in Tables 24 and 25. Line shapes are those characteristic of hot-core emission: widths of ~10 km s^{-1} and central velocities of $v_{LSR} \approx 5$ km s^{-1}. The excitation temperature for both vinyl cyanide and ethyl cyanide is $T_{ex} \approx 150$ K with column densities of 2×10^{14} cm^{-2} and

TABLE 23

TRANSITIONS OF CH_3OCH_3

ν (MHz)	$J_{K_pK_o}$	T_a^* (K)	$\int T_a^* dv$ (K km s^{-1})	Notes
222238.7......	$4_{3,2}-3_{2,1}$ *EA*	0.2	0.8	
222247.5......	$4_{3,2}-3_{2,1}$ *AE*, *EE*	1.3	4.3	
222254.7......	$4_{3,2}-3_{2,1}$ *AA*	1.0	2.6	
222426.8......	$4_{3,1}-3_{2,2}$ *AE*	0.3	1.2	a
222434.0......	$4_{3,1}-3_{2,2}$ *EE*, *AA* }	1.5	4.0	b
222435.6......	$4_{3,1}-3_{2,2}$ *EA* }			
223200.1......	$8_{2,7}-7_{1,6}$ *AE*, *EA* }			
223202.3......	$8_{2,7}-7_{1,6}$ *EE* }	1.1	9.5	
223204.5......	$8_{2,7}-7_{1,6}$ *AA* }			
225598.8......	$12_{1,12}-11_{0,11}$ *EA*, *AE* }			
225599.1......	$12_{1,12}-11_{0,11}$ *EE* }	3.6	12.5	
225599.5......	$12_{1,12}-11_{0,11}$ *AA* }			
226346.0......	$14_{1,13}-13_{2,12}$ *AA* }			
226346.9......	$14_{1,13}-13_{2,12}$ *EE* }	1.6	5.7	
226347.8......	$14_{1,13}-13_{2,12}$ *AE*, *EA* }			
228978.8......	$7_{7,1}-8_{6,2}$ *EA*	0.2	0.6	
228983.2......	$7_{7,1}-8_{6,2}$ *EE* }			
228984.8......	$7_{7,1}-8_{6,2}$ *AE* }			
	$7_{7,0}-8_{6,3}$ *AE* }			
228987.7......	$7_{7,1}-8_{6,2}$ *AA* }	0.2	0.7	
	$7_{7,0}-8_{6,3}$ *AA* }			
228989.3......	$7_{7,0}-8_{6,3}$ *EE* }			
228990.9......	$7_{7,0}-8_{6,3}$ *EA* }			
230465.8......	$10_{8,3}-11_{7,4}$ *EA* }			
230467.8......	$10_{8,3}-11_{7,4}$ *EE* }			
230469.8......	$10_{8,3}-11_{7,4}$ *AA* }			
	$10_{8,2}-11_{7,5}$ *AA* }			
230470.2......	$10_{8,3}-11_{7,4}$ *AE* }	0.4	2.0	
	$10_{8,2}-11_{7,5}$ *AE* }			
230472.2......	$10_{8,2}-11_{7,5}$ *EE* }			
230474.6......	$10_{8,2}-11_{7,5}$ *EA* }			
231987.8......	$13_{0,13}-12_{1,12}$ *AA* }			
231987.9......	$13_{0,13}-12_{1,12}$ *EE* }	3.2	8.3	c
231988.0......	$13_{0,13}-12_{1,12}$ *EA*, *AE* }			
237046.3......	$7_{2,5}-6_{1,6}$ *AE*, *EA* }			
237049.0......	$7_{2,5}-6_{1,6}$ *EE* }	1.5	7.5	d
237051.7......	$7_{2,5}-6_{1,6}$ *AA* }			
237618.9......	$9_{2,8}-8_{1,7}$ *EA*, *AE* }			
237621.0......	$9_{2,8}-8_{1,7}$ *EE* }	0.9	4.8	
237623.0......	$9_{2,8}-8_{1,7}$ *AA* }			
240978.2......	$5_{3,3}-4_{2,2}$ *EA*	0.1	0.4	
240982.9......	$5_{3,3}-4_{2,2}$ *AE* }	1.0	4.1	
240985.2......	$5_{3,3}-4_{2,2}$ *EE* }			
240990.1......	$5_{3,3}-4_{2,2}$ *AA*	0.5	1.0	
241524.0......	$5_{3,2}-4_{2,3}$ *AE*	0.9	4.2	
241528.8......	$5_{3,2}-4_{2,3}$ *EA* }			
241529.0......	$5_{3,2}-4_{2,3}$ *EE* }	1.7	10.2	
241531.2......	$5_{3,2}-4_{2,3}$ *AA* }			
241946.2......	$13_{1,13}-12_{0,12}$ *AE*, *EA* }			
241946.5......	$13_{1,13}-12_{0,12}$ *EE* }	3.8	12.8	
241946.9......	$13_{1,13}-12_{0,12}$ *AA* }			

[a] Blend with $HCOOCH_3$ 222422.
[b] Blend with $HCOOCH_3$ 222439.
[c] Blend with C_2H_5CN 231990.
[d] Blend with SO_2 237069.

2×10^{15} cm^{-2}. Because of its greater column density, emission from ethyl cyanide is much more prominent in the spectrum.

p) *Recombination Lines*

Because of the larger spacing between recombination lines at higher frequencies, only one Hα line falls within our spectral range (see Table 26), in contrast with the four Hα lines observed by Johansson *et al.* (1984). The H30α line at 231901.3 MHz is found to have a peak antenna temperature of 0.7 K, a v_{LSR} of 4 km s^{-1}, and a 23 km s^{-1} line width. The velocity of the emission is somewhat redshifted with respect to that of Johansson *et al.*, although the velocity is not well determined in this measurement. The width is consistent with

TABLE 24

TRANSITIONS OF C_2H_3CN

ν (MHz)	$J_{K_pK_o}$	T_a^* (K)	$\int T_a^* dv$ (K km s^{-1})	notes
216936.7....	$23_{2,22}-22_{2,21}$	0.6	1.3	
218398.5....	$23_{7,17}-22_{7,16}$	0.4 ?	...	a
	$23_{7,16}-22_{7,15}$			
218402.4....	$23_{6,18}-22_{6,17}$			
	$23_{6,17}-22_{6,16}$			
218421.7....	$23_{8,16}-22_{8,15}$	0.3	1.5	
	$23_{8,15}-22_{8,14}$			
218451.3....	$23_{5,19}-22_{5,18}$	0.2	1.4	
218452.3....	$23_{5,18}-22_{5,17}$			
218573.6....	$23_{4,20}-22_{4,19}$	0.3	2.3	
218585.0....	$23_{3,21}-22_{3,20}$	0.3	3.8	
218615.1....	$23_{4,19}-22_{4,18}$	0.2	2.4	
219400.6....	$23_{3,20}-22_{3,19}$	0.3	1.9	
220561.3....	$24_{1,24}-23_{1,23}$	0.4	1.7	
221123.8....	$23_{1,22}-22_{1,21}$	0.4	3.5	
221766.0....	$24_{0,24}-23_{0,23}$	0.4	2.1	
222153.5....	$23_{2,21}-22_{2,20}$	0.4	3.1	
226256.8....	$24_{2,23}-23_{2,22}$	0.2	3.0	
227897.5....	$24_{7,18}-23_{7,17}$	0.5	1.5	
	$24_{7,17}-23_{7,16}$			
227906.6....	$24_{6,19}-23_{6,18}$	0.5	1.9	
	$24_{6,18}-23_{6,17}$			
227918.5....	$24_{8,16}-23_{8,15}$	0.5	2.4	
	$24_{8,17}-23_{8,16}$			
227960.1....	$24_{9,16}-23_{9,15}$	0.5	6.0	
	$24_{9,15}-23_{9,14}$			
227966.0....	$24_{5,20}-23_{5,19}$			
227967.5....	$24_{5,19}-23_{5,18}$			
228090.5....	$24_{3,22}-23_{3,21}$	0.4	2.5	
228104.6....	$24_{4,21}-23_{4,20}$	0.5	3.5	
228160.3....	$24_{4,20}-23_{4,19}$	nd	...	
229087.0....	$24_{3,21}-23_{3,20}$	0.3	2.8	
229647.8....	$25_{1,25}-24_{1,24}$	0.2	1.0	
230487.9....	$24_{1,23}-23_{1,22}$	...	...	b
230738.5....	$25_{0,25}-24_{0,24}$	0.4	3.8	
231952.3....	$24_{2,22}-23_{2,21}$	0.3	2.7	
235563.8....	$25_{2,24}-24_{2,23}$	0.3	4.5	
237397.0....	$25_{7,19}-24_{7,18}$	...	...	c
	$25_{7,18}-24_{7,17}$			
237411.9....	$25_{6,20}-24_{6,19}$	...	...	d
	$25_{6,19}-24_{6,18}$			
237415.4....	$25_{8,18}-24_{8,17}$	0.4 ?	...	d
	$25_{8,17}-24_{8,16}$			
237456.3....	$25_{9,17}-24_{9,16}$	0.2	1.4	
	$25_{9,16}-24_{9,15}$			
237482.8....	$25_{5,21}-24_{5,20}$	0.3	3.1	
237485.0....	$25_{5,20}-24_{5,19}$			
237591.4....	$25_{3,23}-24_{3,22}$	0.4	4.1	
237638.0....	$25_{4,22}-24_{4,21}$	nd	...	
237711.9....	$25_{4,21}-24_{4,20}$	0.3	2.6	
238726.7....	$26_{1,26}-25_{1,25}$	0.2	1.3	
238796.2....	$25_{3,22}-24_{3,21}$	0.2	1.8	
239708.3....	$26_{0,26}-25_{0,25}$	0.1	0.6	
239816.1....	$25_{1,24}-24_{1,23}$	0.5	3.6	
241737.5....	$25_{2,23}-24_{2,22}$	...	...	e
244857.4....	$26_{2,25}-25_{2,24}$	0.5	4.7	
246896.9....	$26_{7,20}-25_{7,19}$	0.5	3.2	
	$26_{7,19}-25_{7,18}$			
246912.2....	$26_{8,19}-25_{8,18}$	...	...	f
	$26_{8,18}-25_{8,17}$			
246918.3....	$26_{6,21}-25_{6,20}$	0.6	4.1	f
	$26_{6,21}-25_{6,19}$			
246952.1....	$26_{9,18}-25_{9,17}$	0.6	1.1	
	$26_{9,17}-25_{9,16}$			

[a] Blend with C_2H_5CN 218390.
[b] Lost under CO 230538.
[c] Blend with $HCOOCH_3$ 237399 and C_2H_5CN 237405.
[d] Blend with C_2H_5CN 237405.
[e] Lost in wings of CH_3OH 241700 and 241767.
[f] Blend with $HCOOCH_3$ 246915.

the lower frequency recombination-line data, and the intensity is comparable with that expected from non-LTE theory for an electron temperature of 10^4 K and a proton emission measure of 10^7 pc cm^{-6}.

The H37β line at 240021.6 MHz and H38β at 222012.2 MHz are not convincingly detected. This is consistent with the noise level in the spectra and the much-reduced intensity expected. The location for the H37β line is contaminated by the presence of an $HCOOCH_3$ line. Similarly, the He30α line is not seen due to its low strength and a competing line of CH_3OCH_3.

q) *Unidentified Lines*

There are at present 27 lines in the spectrum stronger than 0.3 K which are unidentified and which we believe to be real. The frequencies, widths, and peak antenna temperatures of these lines are tabulated in Table 27. All those listed in the table have been individually examined and shown not to be ghosts of lines in the opposite sideband.

r) *Other Species*

Several other species of interest have transitions in this frequency range but have not been convincingly detected. The $J=2-1$ transitions of NO^+ measured by Bowman, Herbst, and De Lucia (1982) are clearly not detected. Similarly, CO^+ is not seen in Orion, since the emission at 236062 MHz can be attributed to $^{13}CH_3OH$, as discussed by Blake *et al.* (1984). The refractory oxides MgO (Steimle, Azuma, and Carrick 1984) and FeO (Endo, Saito, and Hirota 1984) are also not detected, although the limits are not terribly severe and the frequency for MgO is not well determined. Also not seen are the $J=11-10$ transition of $HOCO^+$ and the $3_{1,3}-2_{2,0}$ components of NH_2 (Charo *et al.* 1981).

The nitroxyl radical (HNO) was tentatively identified in Sgr B2 and NGC 2024 by Ulich, Hollis, and Snyder (1977) on the basis of a single line ($1_{0,1}-0_{0,0}$). As far as we know, this assignment has not been verified by observations of other transitions, in part due to the lack of accurate frequency predictions. The frequency of the $3_{0,3}-2_{0,2}$ transition, which

TABLE 25

TRANSITIONS OF C_2H_5CN

ν (MHz)	$J_{K_pK_o}$	T_a^* (K)	$\int T_a^* dv$ (K km s^{-1})	notes
215039.7....	$24_{9,16}-23_{9,15}$	1.1	19.7	
	$24_{9,15}-23_{9,14}$			
215041.9....	$24_{10,15}-23_{10,14}$			
	$24_{10,14}-23_{10,13}$			
215058.0....	$24_{3,22}-23_{3,21}$	1.3	20.6	
215058.6....	$24_{8,17}-23_{8,16}$			
	$24_{8,16}-23_{8,15}$			
215059.2....	$24_{11,13}-23_{11,12}$			
	$24_{11,14}-23_{11,13}$			
215088.2....	$24_{12,13}-23_{12,12}$	0.5	6.7	
	$24_{12,12}-23_{12,11}$			
215109.1....	$24_{7,18}-23_{7,17}$	1.1	9.2	
	$24_{7,17}-23_{7,16}$			
215119.2....	$25_{0,25}-24_{0,24}$	1.0	13.6	
215126.7....	$24_{13,12}-23_{13,11}$	0.5	3.5	
	$24_{13,11}-23_{13,10}$			
215173.3....	$24_{14,11}-23_{14,10}$	0.3	3.9	
	$24_{14,10}-23_{14,9}$			
215211.5....	$24_{6,19}-23_{6,18}$	...	...	a
215212.5....	$24_{6,18}-23_{6,17}$	...	...	a
215400.8....	$24_{5,20}-23_{5,19}$	0.8	15.2	
215428.0....	$24_{5,19}-23_{5,18}$	1.0	18.4	
215620.2....	$24_{4,21}-23_{4,20}$	0.6	12.5	
215941.1....	$6_{4,3}-5_{3,2}$	0.3 ?	...	
215943.1....	$6_{4,2}-5_{3,3}$			
215965.6....	$25_{1,25}-24_{0,24}$	0.3	1.7	
216077.2....	$24_{4,20}-23_{4,19}$	0.7	9.6	
216752.5....	$26_{1,25}-25_{2,24}$	0.3 ?	...	
218390.0....	$24_{3,21}-23_{3,20}$	0.8	9.9	b
219463.6....	$22_{2,21}-21_{1,20}$	0.3	3.3	
219505.6....	$24_{2,22}-23_{2,21}$	0.9	11.5	
220660.9....	$25_{2,24}-24_{2,23}$	0.7	5.4	
222707.2....	$26_{0,26}-25_{1,25}$	0.3	2.9	
222918.2....	$25_{1,24}-24_{1,23}$	0.9	10.6	
223385.3....	$26_{1,26}-25_{1,25}$	0.9	18.7	
223553.6....	$26_{0,26}-25_{0,25}$	0.6	7.9	
223933.7....	$25_{3,23}-24_{3,22}$	0.6	8.1	
224002.1....	$25_{10,15}-24_{10,14}$	0.9	10.8	
	$25_{10,16}-24_{10,15}$			
224003.4....	$25_{9,17}-24_{9,16}$			
	$25_{9,16}-24_{9,15}$			
224017.5....	$25_{11,15}-24_{11,14}$	0.6	9.5	c
	$25_{11,14}-24_{11,13}$			
224028.1....	$25_{8,18}-24_{8,17}$	0.8	8.2	
	$25_{8,17}-24_{8,16}$			
224045.8....	$25_{12,13}-24_{12,12}$	0.3	4.4	
	$25_{12,14}-24_{12,13}$			
224084.3....	$25_{13,12}-24_{13,11}$	0.8	11.4	
	$25_{13,13}-24_{13,12}$			
224088.2....	$25_{7,19}-24_{7,18}$			
	$25_{7,18}-24_{7,17}$			
224131.5....	$25_{14,12}-24_{14,11}$	0.2	2.7	
	$25_{14,11}-24_{14,10}$			
224186.3....	$25_{15,11}-24_{15,10}$	0.2	1.7	
	$25_{15,10}-24_{15,9}$			
224206.6....	$25_{6,20}-24_{6,19}$	0.7	11.8	
224208.1....	$25_{6,19}-24_{6,18}$			
224231.7....	$26_{1,26}-25_{0,25}$	nd	...	
224419.8....	$25_{5,21}-24_{5,20}$	0.4	4.9	
224458.9....	$25_{5,20}-24_{5,19}$	0.7	7.1	
224469.0....	$25_{19,7}-24_{19,6}$	0.3	1.8	
	$25_{19,6}-24_{19,5}$			
224638.7....	$25_{4,22}-24_{4,21}$	0.6	8.4	
224643.3....	$25_{21,4}-24_{21,3}$			
	$25_{21,5}-24_{21,4}$			
225236.1....	$25_{4,21}-24_{4,20}$	0.8	13.7	
227170.2....	$27_{1,26}-26_{2,25}$	nd	...	
227781.0....	$25_{3,22}-24_{3,21}$	0.5	7.9	
228483.1....	$25_{2,23}-24_{2,22}$	0.9	11.9	
228797.5....	$14_{2,12}-13_{1,13}$	0.3	2.1	
229265.2....	$26_{2,25}-25_{2,24}$	0.7	10.7	
231310.4....	$26_{1,25}-25_{1,24}$	0.9	10.6	
231312.3....	$27_{0,27}-26_{1,26}$			
231313.2....	$24_{2,23}-23_{1,22}$			
231854.2....	$27_{1,27}-26_{1,26}$	1.1	11.6	
231990.4....	$27_{0,27}-26_{0,26}$	1.1	17.7	d
232532.3....	$27_{1,27}-26_{0,26}$	nd	...	
232790.0....	$26_{3,24}-25_{3,23}$	1.1	13.7	
232962.3....	$26_{10,16}-25_{10,15}$	1.2	20.0	
	$26_{10,17}-25_{10,16}$			
232967.6....	$26_{9,18}-25_{9,17}$			
	$26_{9,17}-25_{9,16}$			
232975.5....	$26_{11,15}-25_{11,14}$	0.8	10.7	
	$26_{11,16}-25_{11,15}$			
232998.7....	$26_{8,19}-25_{8,18}$	1.1	16.2	
	$26_{8,18}-25_{8,17}$			
233002.7....	$26_{12,15}-25_{12,14}$			
	$26_{12,14}-25_{12,13}$			
233041.1....	$26_{13,14}-25_{13,13}$	0.4	7.7	
	$26_{13,13}-25_{13,12}$			
233069.3....	$26_{7,20}-25_{7,19}$	1.0	12.7	
	$26_{7,19}-25_{7,18}$			
233088.9....	$26_{14,12}-25_{14,11}$	0.5	6.3	
	$26_{14,13}-25_{14,12}$			
233144.8....	$26_{15,11}-25_{15,10}$	0.4	5.6	
	$26_{15,12}-25_{15,11}$			
233205.0....	$26_{6,21}-25_{6,20}$	1.5	21.2	
233207.3....	$26_{6,20}-25_{6,19}$			
233208.1....	$26_{16,10}-25_{16,9}$			
	$26_{16,11}-25_{16,10}$			
233443.1....	$26_{5,22}-25_{5,21}$	0.7	6.9	
233498.3....	$26_{5,21}-25_{5,20}$	0.8	6.7	e
233523.5....	$26_{20,7}-25_{20,6}$	0.5	6.1	f
	$26_{20,6}-25_{20,5}$			
233654.1....	$26_{4,23}-25_{4,22}$	1.1	8.1	g
234423.9....	$26_{4,22}-25_{4,21}$	...	...	h
237170.4....	$26_{3,23}-25_{3,22}$	0.9	10.5	
237360.9....	$28_{1,27}-27_{2,26}$	nd	...	
237405.2....	$26_{2,24}-25_{2,23}$	0.7	10.2	i
237476.0....	$25_{2,24}-24_{1,23}$	0.2 ?	...	
237851.8....	$27_{2,26}-26_{2,25}$	0.4	6.3	
239682.8....	$27_{1,26}-26_{1,25}$	0.7	8.6	j
239887.3....	$28_{0,28}-27_{1,27}$	0.2 ?	...	
240319.3....	$28_{1,28}-27_{1,27}$	0.8	10.5	
240429.2....	$28_{0,28}-27_{0,27}$	0.6	9.4	
240861.3....	$28_{1,28}-27_{0,27}$	0.2 ?	...	
241625.9....	$27_{3,25}-26_{3,24}$	...	...	k
241922.5....	$27_{10,18}-26_{10,17}$	0.9	5.2	
	$27_{10,17}-26_{10,16}$			
241932.2....	$27_{9,19}-26_{9,18}$	1.3	17.4	
	$27_{9,18}-26_{9,17}$			
241933.2....	$27_{11,16}-26_{11,15}$			
	$27_{11,17}-26_{11,16}$			
241959.1....	$27_{12,15}-26_{12,14}$	0.7	5.5	
	$27_{12,16}-26_{12,15}$			

TABLE 25—*Continued*

ν (MHz)	$J_{K_pK_o}$	T_a^* (K)	$\int T_a^* dv$ (K km s^{-1})	notes
241970.4....	$27_{8,20}-26_{8,19}$	0.8	6.8	
	$27_{8,19}-26_{8,18}$			
241997.1....	$27_{13,15}-26_{13,14}$	0.5	3.5	
	$27_{13,14}-26_{13,13}$			
242045.3....	$27_{14,13}-26_{14,12}$	0.8	14.3	
	$27_{14,14}-25_{14,13}$			
242052.4....	$27_{7,21}-26_{7,20}$			
	$27_{7,20}-26_{7,19}$			
242102.2....	$27_{15,13}-26_{15,12}$	0.8	14.4	
	$27_{15,12}-26_{15,11}$			
242167.0....	$27_{16,12}-26_{16,11}$	0.2	1.7	
	$27_{16,11}-26_{16,10}$			
242207.0....	$27_{6,22}-26_{6,21}$	1.3	21.9	
242210.4....	$27_{6,21}-26_{6,20}$			
242238.8....	$27_{17,11}-26_{17,10}$	0.2 ?	...	
	$27_{17,10}-26_{17,9}$			
242470.4....	$27_{5,23}-26_{5,22}$	0.9	12.5	
242547.3....	$27_{5,22}-26_{5,21}$	0.7	7.0	
242664.7....	$27_{4,24}-26_{4,23}$	1.0	12.4	
243643.2....	$27_{4,23}-26_{4,22}$	0.9	13.6	
243823.0....	$26_{2,25}-25_{1,24}$	nd	...	
246268.7....	$27_{2,25}-26_{2,24}$	0.9	6.5	
246421.9....	$28_{2,27}-27_{2,26}$	0.6	5.5	
246548.7....	$27_{3,24}-26_{3,23}$	0.6	5.4	

[a] Lost under SO 215221.
[b] Blend with C_2H_3CN 218399 and 218402.
[c] Blend with $HCOOCH_3$ 224024.
[d] Blend with CH_3OCH_3 231988.
[e] Blend with $HCOOCH_3$ 233505.
[f] Blend with $HCOOCH_3$ 233525.
[g] Blend with $HCOOCH_3$ 233655.
[h] Blend with SO_2 234422.
[i] Blend with C_2H_3CN 237397, 237412, and 237415.
[j] Blend with $CH_3CN(\nu_8)$ 239685.
[k] Lost under SO_2 241616.

TABLE 26

RECOMBINATION LINES

Transition	ν (MHz)	T_a^* (K)	FWHM (km s^{-1})	$T_a^*\, dv$ (K km s^{-1})	v_{LSR} (km s^{-1})
H30α	231901.3	0.7	23.0	15.7	+4.
H38β.......	222012.2	nd	...	...	...
H37β.......	240021.6	nd	...	...	...
He30α	231995.8	nd	...	...	...

falls in this frequency range, has recently been measured to be 244364.0 MHz by Sastry *et al.* (1984). Although a very weak bump is present in Figure 1 at this frequency, it is unclear if this is a real feature or an artifact of the data reduction. At present it is not possible to claim detection of HNO in Orion.

Of considerable interest is the nondetection of ethanol (C_2H_5OH), a structural isomer of the abundant species dimethyl ether (CH_3OCH_3). This indicated a high degree of chemical selectivity in Orion, as previously noted in the Onsala survey (Johansson *et al.* 1984). A similar selectivity holds between acetic acid (CH_3COOH) and methyl formate ($HCOOCH_3$). Although accurate frequencies are not available for acetic acid in this frequency range, if it were as abundant as methyl formate it would be evident through the presence of scores of unidentified lines.

VI. SUMMARY

In this survey we have detected a total of 544 lines from a 32 GHz interval in the spectrum of Orion A. The extraordinary number and strengths of the molecular lines illustrate the importance of studies of line emission from molecular clouds. Line emission is both useful as a key to understanding the kinematic and chemical properties of these clouds and important in its own right as a major factor determining the energy balance within these regions.

As expected, the majority of the lines detected are from heavy asymmetric rotors such as $HCOOCH_3$ and C_2H_5CN. The molecule emitting the largest amount of flux is SO_2, which is also a heavy asymmetric rotor and which in addition has a large column density and is concentrated in the large-line-width plateau source. SO_2 together with the plateau components of CO, CS, and SO account for approximately 70% of the line flux in this frequency range. Most of the lines in the spectrum are readily identified. The few remaining unidentified lines are probably mostly due to the well-studied molecules such as CH_3OH for which it is difficult to make accurate frequency predictions.

The large amount of data reported here is in large part due to the high frequencies at which this survey was conducted. Molecular lines are generally more intense at high frequencies, if they are optically thin and the molecular cloud has sufficiently high excitation. For such higher frequency work it has been necessary to employ more accurate millimeter-wave telescopes. Telescopes of large aperture and high surface accuracy are necessary in order to have narrow beams which will pick out the compact, dense, high-excitation regions such as the Orion plateau source. Also of great importance are sensitive high-frequency receivers. Both will be very important in future high-frequency work. Finally, it is evident that the interpretation of astronomical molecular-line data is near being limited by the amount of available laboratory data, for both well-known molecules and new molecules. Considerable work is needed in obtaining further laboratory data as well as in

TABLE 27

UNIDENTIFIED LINES

ν (MHz)	T_a^* (K)	FWHM (km s^{-1})
215886......	0.9	3.1
217300......	1.2	6.5
217823......	0.7	7.0
217887......	0.9	7.0
222177......	0.4	3.3
222259......	0.6	4.8
222723......	0.6	3.3
224493......	0.5	6.2
224699......	0.7	4.9
224895......	0.7	3.0
225625......	1.0	4.2
226384......	0.5	3.4
226436......	0.4	4.8
227095......	0.9	5.0
227815......	1.4	4.6
229590......	1.3	5.1
230233......	0.6	5.3
232163......	0.8	10.9
234291......	0.6	6.0
235261......	0.5	7.1
236977......	0.9	6.6
237131......	0.7	6.1
238017......	0.4	11.7
239732......	0.6	2.6
242076......	0.7	3.7
243740......	0.8	5.6
243747......	1.1	6.1

theoretical work on line assignments and frequency predictions.

The authors are grateful to F. J. Lovas, H. M. Pickett, F. C. De Lucia, E. Herbst, and G. M. Plummer for providing most of the spectroscopic data used in this work. In addition, the authors would like to thank D. P. Woody and S. L. Scott for their efforts in ensuring successful observations, and R. E. Miller of AT&T Bell Laboratories, Murray Hill, for supplying the junctions used in this work. Single-dish millimeter-wave astronomy at the Owens Valley Radio Observatory is supported by NSF grant AST-8214693.

TABLE 28

KNOWN DEFECTS

ν (MHz)	T_a^* (K)
215136	0.4
215696	1.0
223357	0.6
223378	0.9
232857	0.5
234913	0.5
235217	0.6
243465	0.7
243811	0.9
244411	1.0
245094	0.7
245099	0.6

APPENDIX A

KNOWN DEFECTS IN THE SPECTRUM

The spectrum presented in Figure 1 contains a few noticeable defects arising from the procedure used to generate a single-sideband spectrum from the double-sideband data. The defects are usually in the form of "ghosts," small residuals left when a strong line is not entirely assigned to the proper sideband. Such ghosts will be found separated by approximately twice the IF frequency (a total of ~ 2.5 GHz) from the stronger features in the spectrum. Their reality can usually be checked by examination of the original double-sideband data. All unidentified features in the spectrum stronger than 0.4 K were examined to see if they were ghosts. Those which were found to be real, albeit unidentified, features were listed in Table 27. Those which can be attributed to ghosts are listed below in Table 28.

REFERENCES

Altman, R. S., Crofton, M. W., and Oka, T. 1984, *J. Chem. Phys.*, **80**, 3911.

Blake, G. A., Sutton, E. C., Masson, C. R., Phillips, T. G., Herbst, E., Plummer, G. M., and De Lucia, F. C. 1984, *Ap. J.*, **286**, 586.

Bowman, W. C., Herbst, E., and De Lucia, F. C. 1982, *J. Chem. Phys.*, **77**, 4261.

Charo, A., Sastry, K. V. L. N., Herbst, E., and De Lucia, F. C. 1981, *Ap. J. (Letters)*, **244**, L111.

DeFrees, D. J., McLean, A. D., and Herbst, E. 1984, preprint.

Dickinson, D. F., and Rodriguez-Kuiper, E. N. 1981, *Ap. J.*, **247**, 112.

Endo, Y., Saito, S., and Hirota, E. 1984, *Ap. J. (Letters)*, **278**, L131.

Genzel, R., Downes, D., Ho, P. T. P., and Bieging, J. 1982, *Ap. J. (Letters)*, **259**, L103.

Goldsmith, P. F., Krotkov, R., Snell, R. L., Brown, R. D., and Godfrey, P. 1983, *Ap. J.* **274**, 183.

Goldsmith, P. F., Snell, R. L., Deguchi, S., Krotkov, R., and Linke, R. A. 1982, *Ap. J.*, **260**, 147.

Hollis, J. M., Lovas, F. J., Suenram, R. D., Jewell, P. R., and Snyder, L. E. 1983, *Ap. J.*, **264**, 543.

Hollis, J. M., Snyder, L. E., Blake, D. H., Lovas, F. J., Suenram, R. D., and Ulich, B. L. 1981, *Ap. J.*, **251**, 541.

Irvine, W. M., and Schloerb, F. P. 1984, *Ap. J.*, **282**, 516.

Johansson, L. E. B., *et al.* 1984, *Astr. Ap.*, **130**, 227.

Kawaguchi, K., Saito, S., and Hirota, E. 1983, *J. Chem. Phys.*, **79**, 629.

Linke, R. A., Cummins, S. E., and Thaddeus, P. 1985, in preparation.

Loren, R. B., and Mundy, L. E. 1984, *Ap. J.*, **286**, 232.

Loren, R. B., Mundy, L. E., and Erickson, N. R. 1981, *Ap. J.*, **250**, 573.

Lovas, F. J., Snyder, L. E., and Johnson, D. R. 1979, *Ap. J. Suppl.*, **41**, 451.

Masson, C. R. 1982, *Astr. Ap.*, **114**, 270.

Morris, M., Palmer, P., and Zuckerman, B. 1980, *Ap. J.*, **237**, 1.

Oloffson, H. 1984, *Astr. Ap.*, **134**, 36.

Plummer, G. M., Herbst, E., De Lucia, F. C., and Blake, G. A. 1984, *Ap. J. Suppl.*, **55**, 633.

Plummer, G. M., Herbst, E., De Lucia, F. C., and Blake, G. A. 1985, in preparation.
Poynter, R. L., and Pickett, H. M. 1981, *Submillimeter, Millimeter, and Microwave Spectral Line Catalog* (J.P.L. Pub. 80-23).
Sastry, K. V. L. N., Helminger, P., Plummer, G. M., Herbst, E., and De Lucia, F. C. 1984, *Ap. J. Suppl.*, **55**, 563.
Schloerb, F. P., Friberg, P., Hjalmarson, A., Hoglund, B., and Irvine, W. M. 1983, *Ap. J.*, **264**, 161.
Skatrud, D. D., De Lucia, F. C., Blake, G. A., and Sastry, K. V. L. N. 1983, *J. Molec. Spectrosc.*, **99**, 35.
Steimle, T. C., Azuma, Y., and Carrick, P. G. 1984, *Ap. J.* (*Letters*), **277**, L21.
Sutton, E. C. 1983, *IEEE Trans.*, **MTT-31**, 589.
Sutton, E. C., Blake, G. A., Masson, C. R., and Phillips, T. G. 1984, *Ap. J.* (*Letters*), **283**, L41.
Thorne, L. R., Anicich, V. G., Prasad, S. S, and Huntress, W. T. 1984, *Ap. J.*, **280**, 139.
Ulich, B. L., Hollis, J. M., and Snyder, L. E. 1977, *Ap. J.* (*Letters*), **217**, L105.
Wootten, A., Lichten, S. M., Sahai, R., and Wannier, P. 1982, *Ap. J.*, **257**, 151.
Wootten, A., Loren, R. B., and Bally, J. 1984, *Ap. J.*, **277**, 189.
Wyse, F. C., Manson, E. L., and Gordy, W. 1972, *J. Chem. Phys.*, **57**, 1106.
Zuckerman, B., and Palmer, P. 1975, *Ap. J.* (*Letters*), **199**, L35.

Note added in proof.—Recent laboratory measurements have shown that nine of the lines listed in Table 27 as unidentified are in fact due to methanol (CH_3OH). The measured rest frequencies are 217299.2, 217886.6, 222722.9, 224699.4, 227094.6, 227814.5, 229589.1, 237129.4, and 239731.4 MHz. Relative intensities of the features in the laboratory spectrum are consistent with those in Orion. The total count of unidentified lines is lowered to 18 out of a total of 544 lines.

GEOFFREY A. BLAKE and T. G. PHILLIPS: Downs Laboratory of Physics 320-47, California Institute of Technology, Pasadena, CA 91125

C. R. MASSON: Downs Laboratory of Physics 405-47, California Institute of Technology, Pasadena, CA 91125

E. C. SUTTON: Space Sciences Laboratory, University of California, Berkeley, CA 94720